Impact of dynamical screening on the phonon dynamics of metallic La_2CuO_4

Thomas Bauer and Claus Falter*
Institut für Festkörpertheorie, Westfälische Wilhelms-Universität, Wilhelm-Klemm-Str. 10, 48149 Münster, Germany
(Received 21 August 2008; published 25 September 2009)

It is shown within a quantitative calculation that poor dynamical screening of the long-ranged Coulomb interaction due to the slow charge dynamics around the *c* axis leads in metallic La_2CuO_4 to low-energy electronic collective excitations in a small region around this axis, strongly mixing with certain interlayer phonons. The manifestation of such a phonon-plasmon scenario in layered systems based on a nonadiabatic charge response recently proposed on a qualitative level is quantitatively investigated by a realistic calculation of the frequency and wave-vector-dependent irreducible polarization part of the density response function. Our calculation corrects for a generic deficit of LDA calculations which as a rule predict a too large electronic *c*-axis dispersion insufficient to describe the *c*-axis charge response in general and in particular the phonons along this axis in the cuprates. As shown in this work, the latter are highly sensitive with respect to the interlayer coupling and thus a very accurate electronic dispersion along the *c* axis is crucial. Linear response theory is used to calculate the coupled mode dispersion in the main symmetry directions of the Brillouin zone and the charge-density redistributions excited by certain strongly coupling phononlike and plasmonlike modes. The corresponding mode induced orbital averaged changes in the self-consistent potential felt by the electrons are assessed. Our analysis should be representative for the optimally to overdoped state of the cuprates where experimental evidence of a coherent three-dimensional Fermi surface and a coherent *c*-axis charge transport is given. It is demonstrated that modes from the outside of a small region around the *c* axis can reliably be calculated within the adiabatic limit. On the other hand, modes inside this sector have to be determined nonadiabatically. In particular, the relevance of a strongly coupling nonadiabatic phononlike apex oxygen *Z*-point breathing mode O_z^Z at about 40 meV is emphasized whose mode energy decreases with less doping.

DOI: 10.1103/PhysRevB.80.094525 PACS number(s): 74.72.Dn, 74.25.Kc, 71.45.Gm, 63.20.D−

I. INTRODUCTION

In layered, strongly anisotropic materials such as the copper oxide high-temperature superconductors (HTSCs) the screening of the Coulomb interaction between the layers is imperfect and its dynamic nature becomes important. Perpendicular to the CuO planes low-lying electronic collective modes (interlayer plasmons) can be expected. In connection with superconductivity the interplay between the attractive interaction, mediated, e.g., by phonons, and the dynamically screened Coulomb interaction is more complex than in the conventional theory. Accordingly, the existence and possible relevance of energetically low lying plasmons, e.g., acoustic plasmons, for superconductivity in the cuprates has been discussed before in the literature; see, e.g., Refs. 1–6. A direct observation of low lying plasmons in the HTSCs, e.g., by high-resolution inelastic electron scattering or some other technique is still missing. As shown quantitatively in this work there exists a small **q**-space region around the *c* axis with a nonadiabatic charge response where low lying phonon-plasmon modes can occur. A very high **q**-space resolution would be needed in an experiment to resolve the dispersion. However, there is indirect experimental evidence from different probes, such as the use of reflectance and ellipsometric measurements,[7] external losses in photoemission,[8] infrared reflectivity,[9] or resonant inelastic x-ray scattering.[10]

Concerning *c*-axis transport in a highly anisotropic metal it is interesting to note that in a simplified model treatment the possibility has been pointed out that a strong coupling between electrons and a bosonic mode propagating and polarized in the *c* direction, such as O_z^Z, can lead to a metallic to nonmetallic crossover in the *c*-axis resistivity as the temperature is increased with no corresponding feature in the *xy* plane properties.[11]

A direct experimental search for a phonon-plasmon scenario is inconclusive so far.[12,13] From our calculations in this work we can conclude that much better **q**-space resolution transverse to the *c* axis would be needed in the experiment to resolve the coupled mode dispersion in the small nonadiabatic sector.

A proper account of dynamical screening of the Coulomb interaction is not only substantial for superconductivity, but also for a correct description of normal state properties of the HTSCs such as phonon dynamics along the *c* axis; see our simplified model approach in Refs. 14 and 15 and references therein. In this treatment an eleven-band model that represents approximatively the two-dimensional electronic structure of the CuO plane in terms of the Cu $3d$ and O_{xy} $2p$ orbitals is generalized to the third dimension by introducing a suitable interlayer coupling in parameterized form. By varying this coupling from the outside it is possible to pass from the strictly two-dimensional nonadiabatic soft-plasmon case of the charge response (charge confinement in the CuO plane) to a moderate anisotropic adiabatic situation, typical for DFT-LDA calculations.

These calculations indicate that in a small sector around the *c* axis of metallic La_2CuO_4 phonon-plasmon mixing becomes likely if the interlayer coupling is assumed to be sufficiently weak. Taking the extreme anisotropic limit of this model, i.e., the soft-(*c*-axis)-plasmon case ($\omega_{pl}=0$) we were able to propose a phonon-plasmon scenario and to explain at

least qualitatively an apparent inconsistency between the current interpretation of the INS results for the $\Lambda_1 \sim (0,0,1)$ branches and the infrared data in doped metallic samples of La_2CuO_4 (Refs. 12 and 13). The branches look as expected in adiabatic approximation for a less anisotropic metal, i.e., featuring closed A_{2u} splittings. On the other hand, the infrared data display significant A_{2u} splittings typical for an ionic insulator, even for well doped metallic probes. Such a discrepancy cannot be resolved in LDA-DFT calculations based on the adiabatic approximation.

Now the important questions remain if the phonon-plasmon scenario is at work in real La_2CuO_4 or the other cuprates and what is the effect of doping. These significant topics and their consequences cannot be answered seriously in our earlier model approach and are investigated quantitatively in the present work.

Concerning our earlier investigations important changes and improvements of the present calculations are as follows. The proposed phonon-plasmon scenario in Refs. 14 and 15 is calculated *quantitatively* for La_2CuO_4. In the framework of the assumed soft-plasmon case in Refs. 14 and 15 the characteristic Λ_1 phonon branches which are highly sensitive for probing the correct c-axis coupling of the electrons are not so well described and in particular the Λ_1 branch with the characteristic steep dispersion is completely missing. The calculation in this work based on an improved tight-binding description of the bands cure these problems completely. The results are represented in such a way that a detailed comparison becomes possible with our earlier calculations where the basics of the phonon-plasmon scenario are already given. The doping dependence of the nonadiabatic effects can not be studied reliably with the earlier model approach and is investigated in this paper within a rigid-band approximation. Nonadiabatic phonon-induced charge-density distributions have not been calculated in our earlier model and are investigated in the new model. Finally, the calculated phonon-induced change in the nonadiabatic potential and the corresponding charge fluctuations differ quantitatively and even qualitatively from the results in Ref. 15. Altogether these topics demonstrate that a correct c-axis coupling of the electrons as established in Sec. III A is crucial.

A strong nonlocal, polar electron-phonon coupling results along the c axis together with optical conductivity, also in the well-doped metallic state, because of the poor (dynamical) screening of the Coulomb interaction along this axis. Experimentally this can be seen, for example, by the infrared measurements for metallic La_2CuO_4.[16–19] Direct evidence for the presence and importance of this type of unconventional electron-phonon coupling around the c axis where the electrons in the cuprates are strongly coupled to c-axis polar phonons also comes from a recent study of the self-energy of the nodal quasiparticles in Bi2201 (Ref. 20). For a discussion of phonon-plasmon mixing in the cuprates in the context of many-body polaronic effects in the phonon spectrum, we refer to Ref. 21.

Because of the strong anisotropy of the cuprates and consequently an expected very weak dispersion of the electronic band structure along the c axis, which, however, is systematically overestimated by DFT-LDA calculations, electron dynamics and c-axis phonon dynamics is coupled dynamically and a nonadiabatic treatment with a dynamical screened Coulomb interaction is essential. On the other hand, first-principles calculations[22–25] and also our microscopic calculations, see, e.g., Refs. 15, 26, and 27, have shown that the static DFT is in general a sufficient approximation for phonon modes propagating in the CuO plane of the HTSCs.

An important topic of this paper is to improve the electronic band structure along the c axis. Starting with a realistic tight-binding approximation (TBA) of the first-principles result [31 band model (31BM), Ref. 28] which is as a typical LDA-like band structure not anisotropic enough we adapt the latter to the real anisotropy of the material. To achieve this goal the interlayer coupling is modified to give an optimal description of the c-axis phonons. This is a useful strategy because the latter are highly sensitive probes of the electronic charge response perpendicular to the CuO plane. With such a realistic electronic band structure the wave vector and frequency-dependent irreducible polarization part of the density response function (DRF) is calculated. The latter is used in linear response theory to obtain the dynamically screened Coulomb interaction and ultimately the full nonadiabatic coupled mode dispersion in the main symmetry directions of the Brillouin zone (BZ). Moreover, charge-density redistributions $\delta\rho$ of certain strongly coupling phononlike and plasmonlike modes of the nonadiabatic region and the corresponding mode induced changes in the self-consistent potential δV felt by the electrons are investigated and compared with the adiabatic limit. From our calculations a phonon-plasmon mixing and a strong nonlocal, nonadiabatic polar electron-phonon interaction is predicted for metallic La_2CuO_4. This conclusion should be representative for the optimally to overdoped state of the cuprates where experimental evidence of a coherent three-dimensional Fermi surface (FS) (Ref. 29) and coherent c-axis charge transport is given.[30–32]

The paper is organized as follows. In Sec. II some elements of the theory necessary to understand the calculated results are reviewed. Section III presents the computations. It gives a discussion of the electronic structure and the nonadiabatic mode dispersion. Furthermore, $\delta\rho$ and δV are investigated for certain relevant modes in the cuprates. Finally, a summary of the paper is presented in Sec. IV and the conclusions are drawn.

II. ELEMENTS OF THE THEORY AND MODELING

In the following a brief survey of the theory and modeling is presented. A detailed description can be found in Ref. 33 and, in particular, in Ref. 34 where the calculation of the coupling parameters of the theory is presented.

The local part of the electronic charge response and the electron-phonon interaction (EPI) is approximated in the spirit of the quasi-ion approach[27,35] by an *ab initio* rigid ion model (RIM) taking into account covalent ion softening in terms of (static) effective ionic charges calculated from a tight-binding analysis. The tight-binding analysis supplies these charges as extracted from the orbital occupation numbers Q_μ of the μ (tight-binding) orbital in question

$$Q_\mu = \frac{2}{N}\sum_{n\mathbf{k}} |C_{\mu n}(\mathbf{k})|^2. \quad (1)$$

$C_{\mu n}(\mathbf{k})$ stands for the μ component of the eigenvector of band n at the wave vector $\mathbf{k}$ in the first BZ; the summation in Eq. (1) runs over all occupied states and N gives the number of the elementary cells in the (periodic) crystal.

In addition, scaling of the short-ranged part of certain pair potentials between the ions is performed to simulate further covalence effects in the calculation in such a way that the energy-minimized structure is as close as possible to the experimental one.[36] Structure optimization and energy minimization is very important for a reliable calculation of the phonon dynamics through the dynamical matrix. Taking just the experimental structure data as is done in many cases in the literature may lead to uncontrolled errors in the phonon calculations.

The RIM with the corrections just mentioned then serves as an unbiased reference system for the description of the HTSCs and can be considered as a first approximation for the insulating state of these compounds. Starting with such an unprejudiced rigid reference system nonrigid electronic polarization processes are introduced in form of more or less localized electronic charge fluctuations (CFs) at the outer shells of the ions. Especially in the metallic state of the HTSCs the latter dominate the *nonlocal* contribution of the electronic density response and the EPI and are particularly important in the CuO planes. In addition, *anisotropic* dipole fluctuations (DFs) are admitted in our approach,[34,37] which prove to be specifically of interest for the ions in the ionic layers mediating the dielectric coupling and for the polar modes. Thus, the basic variable of our model is the ionic density which is given in the perturbed state by

$$\rho_\alpha(\mathbf{r}, Q_\lambda, \mathbf{p}_\alpha) = \rho_\alpha^0(r) + \sum_\lambda Q_\lambda \rho_\lambda^{\mathrm{CF}}(r) + \mathbf{p}_\alpha \cdot \hat{\mathbf{r}} \rho_\alpha^{\mathrm{D}}(r). \quad (2)$$

ρ_α^0 is the density of the unperturbed ion, as used in the RIM, localized at the sublattice α of the crystal and moving rigidly with the latter under displacement. The Q_λ and $\rho_\lambda^{\mathrm{CF}}$ describe the amplitudes and the form factors of the CFs and the last term in Eq. (2) represents the dipolar deformation of an ion α with amplitude (dipole moment) $\mathbf{p}_\alpha$ and a radial density distribution ρ_α^{D}. $\hat{\mathbf{r}}$ denotes the unit vector in the direction of $\mathbf{r}$. The $\rho_\lambda^{\mathrm{CF}}$ are approximated by a spherical average of the orbital densities of the ionic shells calculated in LDA taking self-interaction effects (SIC) into account. The dipole density ρ_α^{D} is obtained from a modified Sternheimer method in the framework of LDA SIC.[34] All SIC calculations are performed for the average spherical shell in the orbital averaged form according to Perdew and Zunger.[38] For the correlation part of the energy per electron the parametrization given in Ref. 38 has been used.

The total energy of the crystal is obtained by assuming that the density can be approximated by a superposition of overlapping densities ρ_α. The ρ_α^0 in Eq. (2) are also calculated within LDA SIC taking environment effects, via a Watson sphere potential and the calculated static effective charges of the ions into account. The Watson sphere method is only used for the oxygen ions and the depth of the Watson sphere potential is set as the Madelung potential at the corresponding site. Such an approximation holds well in the HTSCs.[36,39] Finally, applying the pair-potential approximation we get for the total energy

$$E(R,\zeta) = \sum_{\mathbf{a},\alpha} E_\alpha^{\mathbf{a}}(\zeta) + \frac{1}{2}\sum_{(\mathbf{a},\alpha)\neq(\mathbf{b},\beta)} \Phi_{\alpha\beta}(\mathbf{R}_\beta^{\mathbf{b}} - \mathbf{R}_\alpha^{\mathbf{a}}, \zeta). \quad (3)$$

The energy E depends on both the configuration of the ions $\{R\}$ and the electronic (charge) degrees of freedom (EDF) $\{\zeta\}$ of the charge density, i.e., $\{Q_\lambda\}$ and $\{\mathbf{p}_\alpha\}$ in Eq. (2). $E_\alpha^{\mathbf{a}}$ are the energies of the single ions. **a** and **b** denote the elementary cells and α, β the corresponding sublattices. The second term in Eq. (3) is the interaction energy of the system, expressed in terms of *anisotropic* pair interactions $\Phi_{\alpha\beta}$. Both $E_\alpha^{\mathbf{a}}$ and $\Phi_{\alpha\beta}$ in general depend on ζ via ρ_α in Eq. (2).

The pair potentials in Eq. (3) can be separated into long-ranged Coulomb contributions and short-ranged terms; for details see, e.g., Ref. 34.

Using the adiabatic condition, i.e., minimizing $E(R,\zeta)$ with respect to ζ, the electronic degrees of freedom can be eliminated, an expression for the atomic force constants can be given and from this the dynamical matrix in harmonic approximation can be derived as

$$t_{ij}^{\alpha\beta}(\mathbf{q}) = [t_{ij}^{\alpha\beta}(\mathbf{q})]_{\mathrm{RIM}} - \frac{1}{\sqrt{M_\alpha M_\beta}}\sum_{\kappa,\kappa'} [B_i^{\kappa\alpha}(\mathbf{q})]^* [C^{-1}(\mathbf{q})]_{\kappa\kappa'} B_j^{\kappa'\beta}(\mathbf{q}). \quad (4)$$

The first term on the right-hand side denotes the contribution from the RIM. M_α and M_β are the masses of the ions and $\mathbf{q}$ is a wave vector from the first BZ.

The quantities $\mathbf{B}(\mathbf{q})$ and $C(\mathbf{q})$ in Eq. (4) represent the Fourier transforms of the electronic coupling coefficients and are calculated from the energy in Eq. (3), i.e.,

$$\mathbf{B}_{\kappa\beta}^{\mathbf{ab}} = \frac{\partial^2 E(R,\zeta)}{\partial \zeta_\kappa^{\mathbf{a}} \partial R_\beta^{\mathbf{b}}}, \quad (5)$$

$$C_{\kappa\kappa'}^{\mathbf{ab}} = \frac{\partial^2 E(R,\zeta)}{\partial \zeta_\kappa^{\mathbf{a}} \partial \zeta_{\kappa'}^{\mathbf{b}}}. \quad (6)$$

κ denotes the EDF [CF and DF in the present model, see Eq. (2)] in an elementary cell. The **B** coefficients describe the coupling between the EDF and the displaced ions (bare electron-phonon coupling), and the coefficients C determine the interaction between the EDF. The phonon frequencies $\omega_\sigma(\mathbf{q})$ and the corresponding eigenvectors $\mathbf{e}^\alpha(\mathbf{q}\sigma)$ of the modes $(\mathbf{q}\sigma)$ are obtained from the secular equation for the dynamical matrix in Eq. (4), i.e.,

$$\sum_{\beta,j} t_{ij}^{\alpha\beta}(\mathbf{q}) e_j^\beta(\mathbf{q}) = \omega^2(\mathbf{q}) e_i^\alpha(\mathbf{q}). \quad (7)$$

The Eqs. (4)–(7) are generally valid and, in particular, are independent of the specific model for the decomposition of the perturbed density in Eq. (2) and the pair approximation Eq. (3) for the energy. The lengthy details of the calculation of the coupling coefficients **B** and C cannot be reviewed in this paper. They are presented in Ref. 34. In this context we

remark that the coupling matrix $C_{\kappa\kappa'}(\mathbf{q})$ of the EDF-EDF interaction, whose inverse appears in Eq. (4) for the dynamical matrix, can be written in matrix notation as

$$C = \Pi^{-1} + \tilde{V}. \tag{8}$$

Π^{-1} is the inverse of the *irreducible polarization part* of the density response function (matrix) and contains the kinetic part to the interaction C while $\tilde{V}$ embodies the Hartree and exchange-correlation contribution. C^{-1} needed for the dynamical matrix and the EPI is closely related to the (linear) density response function (matrix) and to the inverse dielectric function (matrix) ε^{-1}, respectively.

Only very few attempts have been made to calculate the phonon dispersion and the EPI of the HTSCs using the linear response method in form of density-functional perturbation theory within LDA.[22–24] These calculations correspond to calculating Π and $\tilde{V}$ in DFT-LDA and for the *metallic* state only. On the other hand, in our microscopic modeling DFT-LDA-SIC calculations are performed for the various densities in Eq. (2) in order to obtain the coupling coefficients $\mathbf{B}$ and $\tilde{V}$. Including SIC is particularly important for localized orbitals such as Cu $3d$ in the HTSCs. Our theoretical results for the phonon dispersion,[15,26,37] which compare well with the experiments, demonstrate that the approximative calculation of the coupling coefficients in our approach is sufficient, even for the localized Cu $3d$ states. Written in matrix notation we get for the density response matrix the relation

$$C^{-1} = \Pi(1 + \tilde{V}\Pi)^{-1} \equiv \Pi\varepsilon^{-1}, \quad \varepsilon = 1 + \tilde{V}\Pi. \tag{9}$$

The CF-CF submatrix of the matrix Π can approximatively be calculated for the metallic (but not for the undoped and underdoped) state of the HTSCs from a TBA of a single-particle electronic band structure. In this case the electronic polarizability Π in tight-binding representation reads

$$\begin{aligned}\Pi_{\kappa\kappa'}(\mathbf{q},\omega=0) = -\frac{2}{N}\sum_{n,n',\mathbf{k}} &\frac{f_{n'}(\mathbf{k}+\mathbf{q}) - f_n(\mathbf{k})}{E_{n'}(\mathbf{k}+\mathbf{q}) - E_n(\mathbf{k})} \\ &\times [C^*_{\kappa n}(\mathbf{k}) C_{\kappa n'}(\mathbf{k}+\mathbf{q})] \\ &\times [C^*_{\kappa' n}(\mathbf{k}) C_{\kappa' n'}(\mathbf{k}+\mathbf{q})]^*.\end{aligned} \tag{10}$$

f, E, and C in Eq. (10) are the occupation numbers, the single-particle energies, and the expansion coefficients of the Bloch functions in terms of tight-binding functions.

The self-consistent change in an EDF at an ion induced by a phonon mode $(\mathbf{q}\sigma)$ with frequency $\omega_\sigma(\mathbf{q})$ and eigenvector $\mathbf{e}^\alpha(\mathbf{q}\sigma)$ can be derived in the form

$$\delta\zeta^{\mathbf{a}}_\kappa(\mathbf{q}\sigma) = \left[-\sum_\alpha \mathbf{X}^{\kappa\alpha}(\mathbf{q})\mathbf{u}_\alpha(\mathbf{q}\sigma)\right] e^{i\mathbf{q}\mathbf{R}^{\mathbf{a}}_\kappa} \equiv \delta\zeta_\kappa(\mathbf{q}\sigma) e^{i\mathbf{q}\mathbf{R}^{\mathbf{a}}}, \tag{11}$$

with the displacement of the ions

$$\mathbf{u}^{\mathbf{a}}_\alpha(\mathbf{q}\sigma) = \left(\frac{\hbar}{2M_\alpha\omega_\sigma(\mathbf{q})}\right)^{1/2} \mathbf{e}^\alpha(\mathbf{q}\sigma) e^{i\mathbf{q}\mathbf{R}^{\mathbf{a}}} \equiv \mathbf{u}_\alpha(\mathbf{q}\sigma) e^{i\mathbf{q}\mathbf{R}^{\mathbf{a}}}. \tag{12}$$

The self-consistent response per unit displacement of the EDF in Eq. (11) is calculated in linear response theory as

$$\mathbf{X}(\mathbf{q}) = \Pi(\mathbf{q})\varepsilon^{-1}(\mathbf{q})\mathbf{B}(\mathbf{q}) = C^{-1}(\mathbf{q})\mathbf{B}(\mathbf{q}). \tag{13}$$

A measure of the strength of the EPI for a certain phonon mode $(\mathbf{q}\sigma)$ is provided by the change in the self-consistent potential in the crystal felt by an electron at some space point $\mathbf{r}$, i.e., $\delta V_{\text{eff}}(\mathbf{r},\mathbf{q}\sigma)$. Averaging this quantity with the corresponding density form factor $\rho_\kappa(\mathbf{r}-\mathbf{R}^{\mathbf{a}}_\kappa)$ at the EDF located at $\mathbf{R}^{\mathbf{a}}_\kappa$, we obtain

$$\delta V^{\mathbf{a}}_\kappa(\mathbf{q}\sigma) = \int dV \rho_\kappa(\mathbf{r}-\mathbf{R}^{\mathbf{a}}_\kappa)\delta V_{\text{eff}}(\mathbf{r},\mathbf{q}\sigma) \tag{14}$$

as a parameter for the strength of the EPI in the mode $(\mathbf{q}\sigma)$ mediated by the EDF considered. For an expression of $\delta V^{\mathbf{a}}_\kappa(\mathbf{q}\sigma)$ in terms of the coupling coefficients in Eqs. (5) and (6), see Ref. 15.

The generalization for the quantity Π in Eqs. (8) and (9) needed for the kinetic part of the charge response in the nonadiabatic regime, where dynamical screening effects must be considered, can be achieved by adding $(\hbar\omega + i\eta)$ to the differences of the single-particle energies in the denominator of the expression for Π in Eq. (10). Other possible nonadiabatic contributions to C related to dynamical exchange-correlation effects and the phonons themselves are beyond the scope of the present approach. Using Eq. (9) for the dielectric matrix, ε, and the frequency-dependent version of the irreducible polarization part, Π, according to Eq. (10), the free-plasmon dispersion is obtained from the condition,

$$\det[\varepsilon_{\kappa\kappa'}(\mathbf{q},\omega)] = 0. \tag{15}$$

The coupled-mode frequencies of the phonons and the plasmons must be determined self-consistently from the secular Eq. (7) for the dynamical matrix which now contains the frequency ω implicitly via Π in the response function C^{-1}. Analogously, the dependence on the frequency is transferred to the quantity $\mathbf{X}$ in Eq. (13) and thus to $\delta\zeta_\kappa$ and δV_κ in Eqs. (11) and (14), respectively. Such a nonadiabatic approach is necessary for a description of the interlayer phonons and the charge response within a small region around the c axis as performed in this work.

The time-consuming numerical calculations were carried out on the computers of the Morfeus GRID at the Westfälische Wilhelms-Universität Münster, with the use of Condor.[40]

III. RESULTS AND DISCUSSION

A. Model of the single-particle content of the irreducible polarization part

As a first approximation the electronic band structure (BS) $E_n(\mathbf{k})$ of La_2CuO_4 and the expansion coefficients $C_{\kappa n}(\mathbf{k})$, needed as input for the single particle content of the

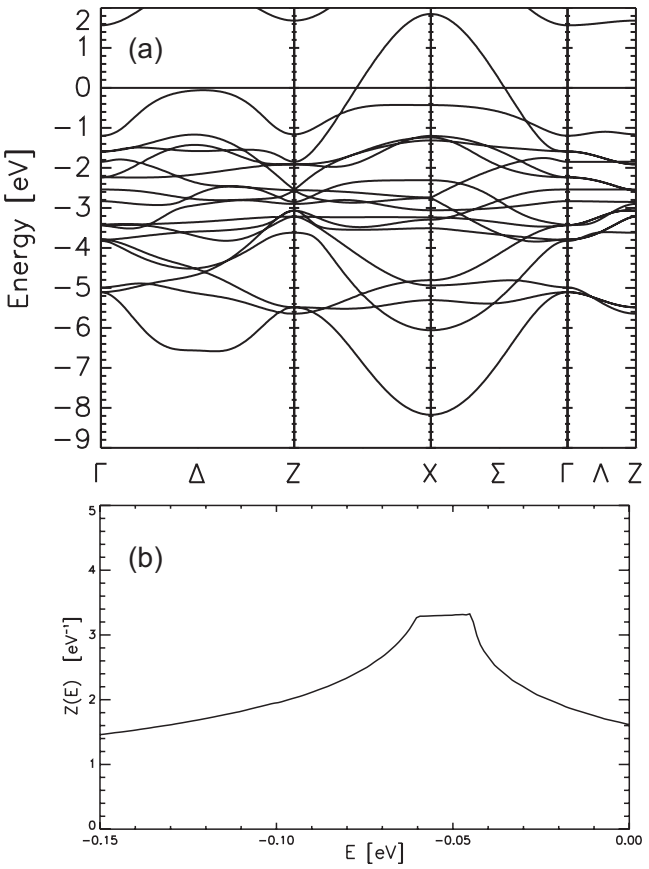

FIG. 1. Electronic band structure $E_n(\mathbf{k})$ of La_2CuO_4 in the 31BM obtained from an accurate tight-binding representation of the first-principles linearized augmented-plane-wave band structure (Ref. 28). (a) The Fermi energy E_F corresponding to the undoped material is taken as the zero of the energy. (b) Density of states $Z(E)$ of the 31BM.

irreducible polarization part $\Pi_{\kappa\kappa'}$ in Eq. (10) are taken from an accurate tight-binding representation of the first-principles linearized augmented-plane-wave band structure (LAPW) as obtained within the framework of DFT LDA.[28]

This analysis leads to a 31BM including the La $5d$, Cu $3d$, $4s$, $4p$, and O $2p$ states. The result for the recalculated tight-binding band structure is shown in Fig. 1(a) and the corresponding density of states (DOS)

$$Z(E) = \frac{2}{N}\sum_{n\mathbf{k}} \delta[E_n(\mathbf{k}) - E] \tag{16}$$

is displayed in Fig. 1(b). The van Hove peak in the DOS is broadened by the dispersion of the band structure in c direction.

The corresponding calculated phonon dispersion of La_2CuO_4 in the adiabatic approximation for the Λ_1 modes polarized along the c axis being most sensitive with respect to the interlayer coupling is presented in Fig. 2(a). The open squares indicate the present "interpretation" in the literature of the experimental results.[12,13] This interpretation will be discussed in detail in Sec. III B. The characteristic experimental features of the dispersion are the steplike structure of

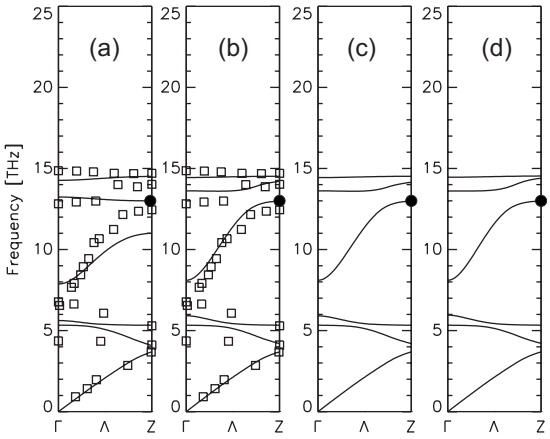

FIG. 2. Calculated phonon dispersion for metallic La_2CuO_4 in the adiabatic approximation for the c-axis polarized Λ_1 modes [$\sim(0,0,1)$] based on the band structure within the 31BM as input for the proper polarization part $\Pi_{\kappa\kappa'}$ (a). (b)–(d) calculated Λ_1 modes as in (a) but using the modified 31BM (M31BM) as discussed in the text as input for $\Pi_{\kappa\kappa'}$. The panels (b)–(d) represent the phonon dispersion for three different doping levels $x=0.156(E_F=-0.08)$, $0.224(E_F=-0.10)$, and $0.297(E_F=-0.135)$, by applying a rigid-band approximation of the M31BM to represent the optimally doped to overdoped state of La_2CuO_4. The experimental results (open squares □) are taken from Refs. 12 and 13. The full dot (●) denotes the O_z^Z mode. E_F is in units of eV.

the second highest branch and most significant the third highest branch with the steep dispersion from the Γ point towards the Z point. Both features are not well reflected in the calculation based on the typical DFT-LDA-like band structure of the 31BM which underlies the computation of the static ($\omega=0$) proper polarization part $\Pi_{\kappa\kappa'}$ in Eq. (10). As we see in a moment, the reason for this is an overestimation of the residual k_z dispersion of the bands, i.e., the DFT-LDA-like band structure is not anisotropic enough. It should be remarked that an earlier calculation within the 31BM (Ref. 41) neglecting dipole fluctuations as additional electronic polarization processes besides the charge fluctuations still further enhances the deviations between the calculated and the measured result for the Λ_1 modes. Anisotropic DF's being particular important along the c axis and for ions in the ionic layers[37] have been taken into account in the calculations shown in Fig. 2(a) and in all other computations of the phonon dispersion presented in this paper.

In order to improve the LDA-like electronic BS of the 31BM which overestimates the c-axis coupling we have investigated the effect on the Λ_1 modes of a modification of the tight-binding parameters of the 31BM. It turns out that a reduction in the first neighbor O_{xy}-La parameters by 1/6 and of the first neighbor La-La parameters by 1/3 leads to a much better result for the calculated Λ_1 modes in adiabatic approximation; see Figs. 2(b)–2(d). The latter results have been obtained for three different doping levels, where the effect of alloying was treated in rigid-band approximation by lowering the Fermi level appropriately to accommodate x holes per primitive cell.

The modified electronic BS of La_2CuO_4 and the corresponding DOS is shown in Figs. 3(a) and 3(b), respectively.

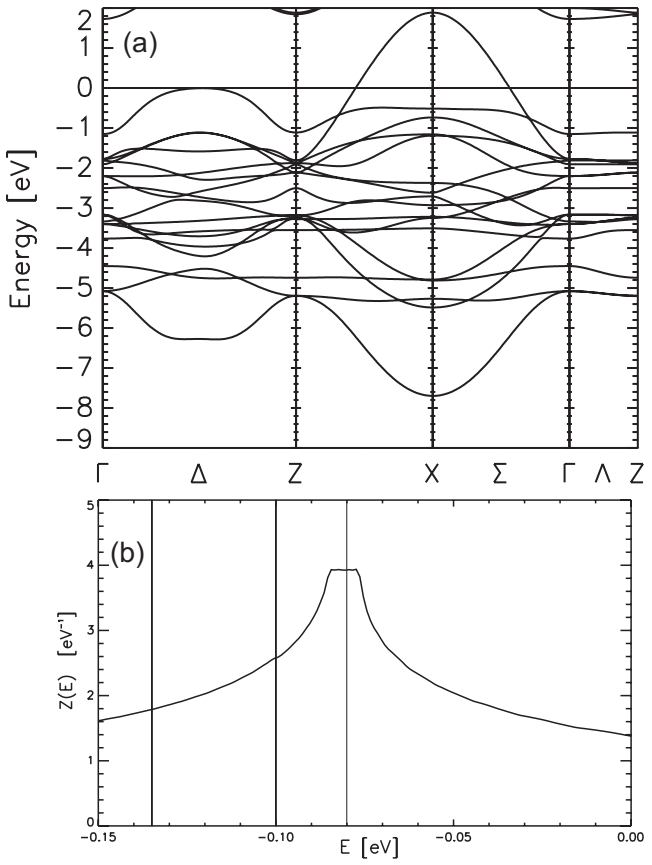

FIG. 3. (a) Electronic band structure $E_n(\mathbf{k})$ of La_2CuO_4 in the M31BM taking into account the enhanced anisotropy of the real material as compared with the 31BM typical for LDA. (b) Density of states $Z(E)$ in the M31BM. The vertical lines indicate the different doping levels from optimal to overdoping as in Fig. 2.

The calculated phonon dispersion is now in good agreement with the experiment. In particular the characteristic features, i.e., the Λ_1 branch with the steep dispersion and the steplike behavior are well described. Moreover, we find as a consequence of the enhanced anisotropy a rearrangement of the three Z-point modes with the highest frequencies. While in the 31BM the anomalous O_z^Z mode is the second highest mode, in the more anisotropic modified 31BM (M31BM) with a weaker coupling along the c axis, O_z^Z is the lowest of the three modes and the end point of the steep branch.

From a comparison of the BS of the 31BM in Fig. 1(a) with the BS of the M31BM in Fig. 3(a) we extract that in the latter case the saddle point region around $\Delta/2$ is more extended and the width of the BS is reduced by about 0.5 eV in the energy range shown in the figure. Important for the charge response along the c axis is the decrease in the k_z dispersion of the bands along the Λ direction. The calculated reduction in the k_z dispersion of the electronic band structure between the LDA result (31BM) and the modified LDA result (M31BM) is illustrated in Fig. 4. The related difference in energy is 17.5 meV for the 31BM but only 9.6 meV for the M31BM, respectively. From this result we extract that very small changes in energy for the k_z dispersion are very important for the phonons propagating along the c axis in La_2CuO_4 and probably also for the c-axis phonons in the other cuprates. Thus theoretical calculations of the electronic band structure along the c axis have to be extremely accurate to describe the real materials.

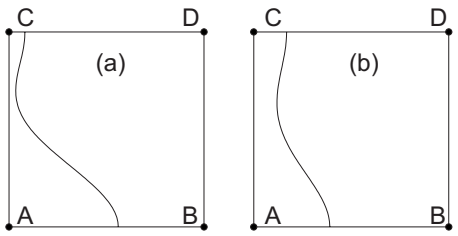

FIG. 4. Electronic k_z dispersion for La_2CuO_4 along the cut of the Fermi surface highlighted in Fig. 6(a) by the black bar. (a) 31BM and (b) M31BM. The corners of these surfaces are A $=(0.4\frac{2\pi}{a},0.05\frac{2\pi}{a},0)$, B $=(0.5\frac{2\pi}{a},0.05\frac{2\pi}{a},0)$, C $=(0.4\frac{2\pi}{a},0.05\frac{2\pi}{a},\frac{2\pi}{c})$, and D $=(0.5\frac{2\pi}{a},0.05\frac{2\pi}{a},\frac{2\pi}{c})$.

Comparing the calculated results for the DOS in both models, see Figs. 1(b) and 3(b), respectively, we find that the broadening of the van Hove peak is decreased in the M31BM by about 50% because of the reduced k_z dispersion. Simultaneously, the DOS $Z(E)$ around the peak is enhanced by the increased anisotropy. This result demonstrates that the correct c-axis anisotropy is very important in influences the properties of the normal and superconducting states of the cuprates via $Z(E_F)$.

Another important effect of the weakening of the interlayer coupling in our modeling as compared to a typical DFT-LDA band structure, leading to a significant enhancement of the DOS $Z(E_F)$ at the Fermi energy E_F, is the amplification of the proper polarization part $\Pi_{\kappa\kappa'}(\mathbf{q})$ on his part. This can be seen in the long-wavelength limit where the sum rule

$$\lim_{\mathbf{q}\to\vec{0}}\sum_{\kappa\kappa'}\Pi_{\kappa\kappa'}(\mathbf{q}) = Z(E_F) \tag{17}$$

rigorously holds for a metal.[33] Altogether, the results demonstrate the importance of a correct interlayer coupling for the electronic properties in the cuprates.

The vertical lines in Fig. 3(b) indicate three doping levels x in rigid-band approximation. The specific dopings have been selected to model the optimally doped state of La_2CuO_4 with the Fermi energy E_F at the van Hove peak (model OP: $E_F=-0.08$ eV, $x=0.156$) and two overdoped states (model OD1: $E_F=-0.10$ eV, $x=0.224$; model OD2: $E_F=-0.135$ eV, $x=0.297$).

The doping levels chosen in this way allow for a comparison of measured FSs at these levels[42,43] with the calculated FS within the M31BM; see Fig. 5. From the comparison we conclude that the overall features of the BS calculation in the M31BM are in good agreement with the results obtained by angle-resolved photoemission spectroscopy (ARPES) over the doping range considered. Such an agreement obtained within the M31BM and the consistence with the Λ_1 phonons speaks in favour of this model with renormalized c-axis hopping parameters leading to an enhanced anisotropy. Moreover, it demonstrates the importance of an experimental verification of a computed electronic band structure. Clearly

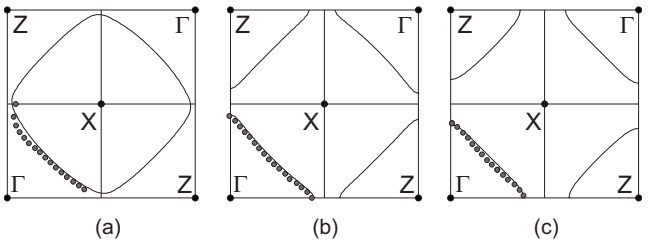

FIG. 5. Comparison of the doping evolution of the measured Fermi surface of $La_{2-x}Sr_xCuO_4$ from Refs. 42 and 43 for optimal doping ($x=0.15$) to overdoping ($x=0.22;0.30$) with the corresponding calculated Fermi surface within the rigid-band approximation of the M31BM, respectively. The dots indicate the experimental results.

visible in the experiments and the calculations is the change in the FS topology and of the related nesting structures upon doping when passing from the model OP to model OD1 or OD2, respectively.

Strong nesting of the FS can bring about either a charge-density wave or a spin density wave, or possibly both. The tendency toward Fermi-surface-driven instabilities frequently is announced by maxima of the so-called (noninteracting) susceptibility

$$\Pi_0(\mathbf{q}) = -\frac{2}{N}\sum_{\substack{n,n' \\ \mathbf{k}}} \frac{f_{n'}(\mathbf{k}+\mathbf{q}) - f_n(\mathbf{k})}{E_{n'}(\mathbf{k}+\mathbf{q}) - E_n(\mathbf{k})}, \tag{18}$$

which can be obtained form Eq. (10) by equating all the expansion coefficients $C_{\kappa n}(\mathbf{k})$ to one. It is obvious from this form that possible FS nesting at certain $\mathbf{q}$ vectors is reflected as a maximum of this function.

From inspection of the FS in Fig. 5 we can expect that approximate nesting vectors around the X point of the BZ will lead to corresponding maxima in $\Pi_0(\mathbf{q})$. For the optimally doped case (model OP) we find a maximum at the X point and in the overdoped state (models OD1 and OD2) the maximum is progressively shifted toward the Γ point. The position of the maximum for model OP is significant because it coincides with the ordering wave vector in the antiferromagnetic state. For the overdoped state, the ordering wave vector (magnetic scattering peak) is predicted from our calculations for Π_0 to move inward from the X point towards the Γ point. Quite general, in the doped cuprates the spin fluctuations (SFs) are antiferromagnetic in origin and arise from both, nesting properties of the FS (spin-density-wave-type SFs) and from correlation driven nearest-neighbor antiferromagnetic superexchange because of the proximity of a long-range ordered antiferromagnetic state in the undoped parent compounds.

In Fig. 6 we display for the models OP, OD1, and OD2 FS maps for different k_z values ($k_z=0, k_z=\frac{2\pi}{c}$) as a function of $\mathbf{k}=(k_x,k_y)$. This allows, for example, to map the k_x and k_y dependence of the c-axis dispersion. The calculations demonstrate that the effect of the k_z dispersion vanishes along the nodal direction and that it increases as one moves towards the antinodal region. The three dimensionality associated with the k_z dispersion (compare with Fig. 4), usually neglected in discussing the physics of the cuprates, also has been shown to play a key role in shaping the ARPES spectra,[30,44] because the residual k_z dispersion of bands in a quasi-two-dimensional material will induce an irreducible linewidth in ARPES peaks. On the other hand detecting such k_z related linewidth in the ARPES spectra as found for La_2CuO_4 (Ref. 30) establishes the existence of coherent c-axis transport.

Finally, to get also a more global impression of the magnitude of the enhanced anisotropy in the M31BM as compared with a typical DFT-LDA-based first-principles result, we compare some FS parameters being important for transport properties such as the Drude plasma energy tensor and the Fermi velocity tensor. The Drude tensor is defined as

$$\hbar\Omega_{p,ij} = \left\{ \frac{8\pi}{NV_z} \sum_{\mathbf{k}n} \delta[E_n(\mathbf{k}) - E_F] v_{\mathbf{k}n,i} v_{\mathbf{k}n,j} \right\}^{1/2}, \tag{19}$$

and the Fermi velocity tensor is given by

$$\langle v^2_{F,ij} \rangle^{1/2} = \left\{ \frac{2}{N} \sum_{\mathbf{k}n} \Theta[E_n(\mathbf{k}) - E_F] v_{\mathbf{k}n,i} v_{\mathbf{k}n,j} \right\}^{1/2}, \tag{20}$$

with

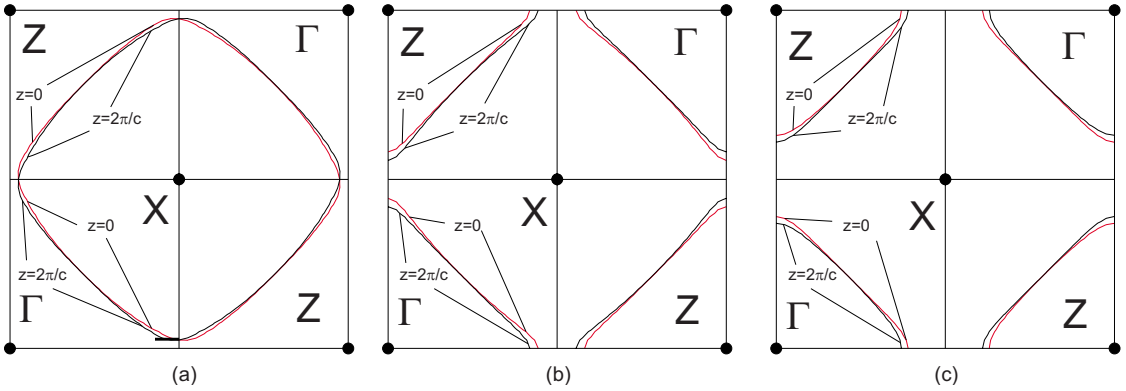

FIG. 6. (Color online) Fermi-surface maps for different k_z values ($k_z \equiv z=0$ and $k_z \equiv z=\frac{2\pi}{c}$) as a function of $\mathbf{k}_\parallel=(k_x,k_y)$ for different doping levels in rigid-band approximation of the M31BM. (a) Model OP ($x=0.156$), (b) model OD1 ($x=0.224$), and (c) model OD2 ($x=0.297$). For the explanation of the small black bar in (a) see Fig. 4.

TABLE I. Comparison of the Fermi-surface parameters (Drude plasma energy tensor, Fermi velocity) and the anisotropy ratios $A_\Omega=\Omega_{p,xx}/\Omega_{p,zz}$; $A_{v_F}=\langle v^2_{F,xx}\rangle^{1/2}/\langle v^2_{F,zz}\rangle^{1/2}$ for optimally doped La_2CuO_4 between a calculation in LAPW (Refs. 45 and 46) and the M31BM (model OP), respectively. $\Omega_{p,ij}$ is given in units of THz and the Fermi velocity $\langle v^2_{F,ij}\rangle^{1/2}$ in units of 10^7 cm/s.

	$\hbar\Omega_{p,xx}$	$\hbar\Omega_{p,zz}$	$\langle v^2_{F,xx}\rangle^{1/2}$	$\langle v^2_{F,zz}\rangle^{1/2}$	A_Ω	A_{v_F}
LAPW	701.21	132.99	2.20	0.41	5.27	5.37
OP	648.60	25.25	2.99	0.11	25.69	27.97

$$\mathbf{v}_{\mathbf{k}n}=\frac{1}{\hbar}\frac{\partial E_n(\mathbf{k})}{\partial \mathbf{k}}. \tag{21}$$

The outcome from our model OP for the optimally doped state is compared in Table I with the corresponding results calculated for optimally doped La_2CuO_4 within LAPW.[45,46] From the table we extract an enhancement of the anisotropy ratio $A_\Omega=\Omega_{p,xx}/\Omega_{p,zz}$ and of $A_{v_F}=(v^2_{F,xx})^{1/2}/(v^2_{F,zz})^{1/2}$ by about a factor 5 in the M31BM as compared to the LAPW calculation.

B. Nonadiabatic phonon calculations and phonon-plasmon coupling

We prelude this section with a discussion of the anomalous behavior of the apex-oxygen bond-stretching mode in metallic La_2CuO_4 at the Z point of the BZ (O_z^Z) polarized perpendicular to the CuO plane. From the experimental side, it took quite some time until this mode could be assessed[13] because of a massive line broadening of about 4 THz in the metallic phase at optimal doping and its very large softening of about 5.5 THz when passing from the insulating to the metallic state.[12,13] The strong softening of this mode across the insulator-metal transition was predicted prior to the experimental observation; see Refs. 26, 33, and 36.

Optical modes such as O_z^Z are of special importance for the cuprates because of their strong *nonlocal* polar coupling to the electrons due to the long-ranged Coulomb interaction poorly screened along the c axis in these compounds, even in the metallic state. As a consequence nonlocal, nonadiabatic polar electron-phonon coupling effects become substantial. These high-frequency c-axis polarized optical phonons are basically unscreened. Quite recently such a long-ranged polar EPI has been identified as very essential also for pairing in the cuprate superconductors.[47,48] The manifestation of the coupling between electrons and polar c-axis phonons in the self-energy of the nodal quasiparticles in Bi2201 has been pointed out recently in Refs. 20 and 49.

Displacements of the ions in the *ionic layers* of the cuprates, in particular those of the O_z^Z mode, bring about large changes in the potential felt by the electrons (holes) in the *CuO plane*, especially in the nonadiabatic phonon-plasmon regime; see, e.g., Table III. On the other hand, it is a fact that the electrons in the CuO plane, shown by our calculations to be strongly nonlocally coupled to the phonon dynamics of the ionic layers, are responsible for the superconductivity and the unusual normal state effects in the cuprates. So, the c-axis polarized optical phonons become important for the renormalization of the electrons in the CuO plane, besides the renormalization due to strong correlation effects. Thus, both, the short-ranged and the long-ranged part of the Coulomb interaction is significant for the physics in the HTSCs, see also Ref. 48, where it is found that a proper combination of strong electron correlation with a poorly screened long range EPI is a possible origin of high-temperature superconductivity in the cuprates.

In the insulating parent compound O_z^Z is found at about 17 THz while in the optimally doped material the experimental value is estimated at about 11.5 THz.[12] However, the large linewidth of about 3–4 THz[12,13] and the presence of another Z-point mode at about 14 THz makes it difficult to pin down the exact position of O_z^Z in the metallic phase.

In the following we will demonstrate within the M31BM that due to the nonlocal, nonadiabatic charge response two coupled phonon-plasmon modes of O_z^Z type arise at 9.09 and 13.86 THz, respectively, and that we can attribute to O_z^Z an *adiabatic* frequency of 12.96 THz. Before discussing these results in more detail we present in retrospect a short explanation of the large softening of O_z^Z during the insulator-metal transition; for details see, e.g., Ref. 26 and earlier references therein.

In the insulating state O_z^Z can be shown to induce only an *intralayer* charge transfer between the copper and oxygen orbitals such that local charge neutrality of the cell is maintained under a perturbation due to O_z^Z. In this way the charge rearrangement leading to screening is considerably restricted and thus we find a high calculated frequency of O_z^Z in the insulating state in agreement with experiment. Contrarily, in the metallic state no such restriction is present and O_z^Z generates CF's at Cu and O_{xy} that have the same sign in the whole CuO layer. This ultimately leads to an (instantaneous) interlayer charge transfer in adiabatic approximation which provides an effective screening mechanism for the long-ranged Coulomb interaction and produces the anomalous softening of O_z^Z during the insulator-metal transition in the calculations consistent with the measurements. Eventually, the instantaneous interlayer charge transfer in the adiabatic approximation is replaced by a collective dynamic charge transfer within the phonon-plasmon scenario in a small region around the c axis, including of course the Z point. Such a scenario will be investigated next within the M31BM.

In Fig. 7 we present our results of the dispersion of the coupled phonon-plasmon modes in the small region around the c axis characterized by a nonadiabatic charge response introducing doping in rigid-band approximation. Within our earlier model the doping dependence of nonadiabatic effects cannot be performed reliably and different interlayer couplings had to be assumed to simulate doping. In Fig. 7 we

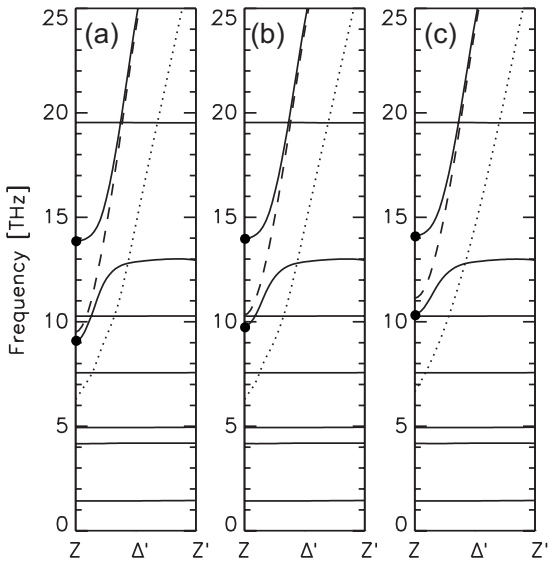

FIG. 7. Calculated coupled phonon-plasmon dispersion of the Δ_1', ($O_z^{Z'}$) modes (—) from the Z point ($\varepsilon=0$) along $\Delta'=(\varepsilon\frac{2\pi}{a},0,\frac{2\pi}{c})$ to $\varepsilon=0.02(Z')$ for the models (a) OP, (b) OD1, and (c) OD2, respectively. The coupling O_z^Z modes at Z are represented by ●; – –: free plasmon branch; ⋯ borderline for damping due to electron-hole decay.

have calculated the coupled mode dispersion of the Δ_1' modes from $Z=(0,0,\frac{2\pi}{c})$ along Δ' to $Z'=(\varepsilon\frac{2\pi}{a},0,\frac{2\pi}{c})$ with $\varepsilon=0.02$. The mixed mode dispersion in Fig. 7(a) is for the optimally doped case of La_2CuO_4 (model OP). Figures 7(b) and 7(c) show the results for the overdoped material, i.e., for model OD1 and OD2, respectively. The strongly coupling O_z^Z modes are indicated as full dots. The broken line is the dispersion of the free-plasmon branch, calculated from Eq. (15) and the dotted line is the borderline for damping due to electron-hole decay, i.e., $\max_{\mathbf{k}\in BZ}[E_n(\mathbf{k})-E_n(\mathbf{k}+\mathbf{q})]$ for the band crossing the Fermi level. We observe a slight increase in the frequency of the free-plasmon branch upon doping which indicates a small reduction in the anisotropy in the overdoped state.

The phonon-plasmon scenario is exemplified for optimally doped La_2CuO_4 in Fig. 7(a). From inspection of the figure we can learn two important facts. Firstly, the range of the region in $\mathbf{q}$ space with a nonadiabatic charge response can be estimated and, secondly, the massive line broadening of the O_z^Z mode can be understood. The full dots at the Z point are the phononlike and plasmonlike O_z^Z(na) mode at 9.09 and 13.86 THz, respectively. We denote the lower mode as phononlike because this mode connects to the adiabatic $O_z^{Z'}$(ad) phonon in the adiabatic region. $O_z^{Z'}$(ad) has virtually the same frequency as the O_z^Z(ad) mode calculated in adiabatic approximation, i.e., O_z^Z(ad)=12.96 THz. From the figure we can extract that the region of nonadiabatic charge response, characterized by the steep phononlike branch is very small. It can be estimated at about $\varepsilon\approx0.01$.

The plasmonlike branch starts at the higher O_z^Z(na) mode, rapidly leaves the frequency range of the phonon spectrum within the nonadiabatic region and becomes more and more plasmonlike as it approaches the free-plasmon dispersion. The experimentally measured massive line broadening for O_z^Z of about 3–4 THz[12,13] in the optimally doped probe can be understood from the calculated phonon-plasmon scenario displayed in Fig. 7(a). Experimentally, there is a limited wave-vector resolution in the transverse direction perpendicular to the c axis which is on average $\varepsilon\approx0.03$ (Ref. 50). Thus, the relevant frequency range sampled by the neutron scattering experiment is over the steep branch and is between the two nonadiabatic O_z^Z(na) modes leading to an estimated broadening of about 3.9 THz. Because the region with a metallic, adiabatic charge response outweighs by a factor of three the nonadiabatic region we can attribute to the broad O_z^Z mode an adiabatic frequency of about 12.9 THz.

The calculated character of the coupled modes along Δ' can be obtained from Table II where the displacement amplitudes for the phononlike and plasmonlike modes are given in terms of relative displacements of the apex oxygen O_z and the La ion along the c axis. At the Z-point O_z and La are vibrating in phase for the phononlike mode and out of phase for the plasmonlike mode. In case of the phononlike mode the amplitude of O_z^Z remains more or less constant while the amplitude for La decreases with increasing ε and finally runs out of phase with O_z in the adiabatic region. In the plasmonlike O_z^Z mode the O_z and La ions always vibrate out of phase. Increasing ε the amplitude of O_z^Z decreases while the magnitude of the amplitude of La increases. The different phase relation of the two modes is reflected in the corresponding induced charge redistributions as discussed below.

The size $\varepsilon\approx0.01$ of the nonadiabatic region predicted by our calculation within model OP is too small for an experi-

TABLE II. Calculated displacement amplitudes of the phononlike and plasmonlike $O_z^{Z'}$ modes in model OP along the $\Delta'=(\varepsilon\frac{2\pi}{a},0,\frac{2\pi}{c})$ direction between $\varepsilon=0$ (Z point) and $\varepsilon=0.02$. The frequency is given in units of THz. The leftmost data set is the result for O_z^Z in the adiabatic limit. The plasmonlike mode for $\varepsilon=0.02$ has not been calculated because its frequency is far out of the relevant frequency range; see Fig. 7(a).

ε	Z(ad)	Z(na)	0.001	0.003	0.004	0.007	0.01	0.02
ω	12.96	9.09	9.27	10.59	11.41	12.61	12.86	12.94
$O_z(z)$	0.69	0.66	0.67	0.70	0.71	0.69	0.69	0.69
La(z)	−0.15	0.25	0.22	0.05	−0.04	−0.13	−0.15	−0.15
ω	12.96	13.86	13.90	14.28	14.81	18.69	24.38	
$O_z(z)$	0.69	0.68	0.68	0.67	0.67	0.61	0.59	
La(z)	−0.15	−0.20	−0.20	−0.22	−0.24	−0.33	−0.38	

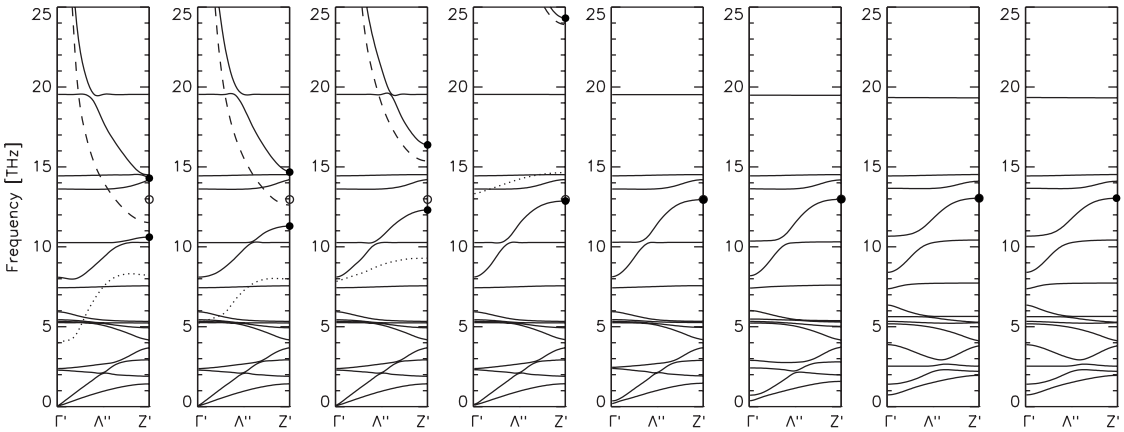

FIG. 8. Nonadiabatic coupled phonon-plasmon dispersion as calculated with model OP for the proper polarization part, representing the optimally doped state of La_2CuO_4 from $\Gamma'=(\varepsilon\frac{2\pi}{a},0,0)$ to Z' along the $\Lambda''=(\varepsilon\frac{2\pi}{a},0,\zeta\frac{2\pi}{c})$ direction. In the different panels of the figure from left to right the following values of ε have been used: $\varepsilon=0.003,0.004,0.006,0.01,0.025,0.05,0.100$. The rightmost panel shows the results of a calculation in adiabatic approximation for $\varepsilon=0.100$. Only the Λ'' branches (—) coupling to the charge fluctuations are shown. – –: free-plasmon branch; ⋯: borderline for damping. Dots at Z': ● $O_z^{Z'}$(na); ○ $O_z^{Z'}$(ad). na: nonadiabatic; ad: adiabatic.

mental observation of the dispersion of the coupled phonon-plasmon modes shown in Fig. 7. Only sampling the nonadiabatic region on average as mentioned above seems possible at present.

Inspection of Figs. 7(b) and 7(c) for the overdoped states leads to about the same size of the nonadiabatic sector as in the optimally doped case and to the same adiabatic frequency for $O_z^{Z'}$(ad) and O_z^{Z}(ad), respectively. However, the broadening of O_z^{Z} is predicted by the calculation to decrease as compared to the optimally doped case. A decrease in the linewidth of O_z^{Z} with practically no change in the frequency has also been found quite recently for overdoped La_2CuO_4 in the experiments.[51] Thus, our prediction within the rigid-band approximation is conform with the measurements. From Figs. 7(b) and 7(c) the width of O_z^{Z} is 3.23 THz for $x\approx0.22$ and 2.66 THz for $x\approx0.3$, respectively. Last but not least we can read off from Fig. 7 a doping dependence of the phononlike O_z^{Z} mode in which the mode energy decreases with reduced doping (OD2: 10.31 THz; OD1: 9.74 THz; and OP: 9.09 THz).

Now we comment on the present interpretation of the measured dispersion of the steep Λ_1 branch displayed in Fig. 2. We just have shown through our calculation of the phonon-plasmon dispersion along the Δ' direction that the nonadiabatic region around the c axis is so small that it cannot be resolved by the INS experiments and only an average of the dispersion can be measured. So, we investigate in detail the coupled mode dispersion along the two directions $\Lambda''=(\varepsilon\frac{2\pi}{a},0,\zeta\frac{2\pi}{c})$ in Fig. 8, $\zeta\in[0,1]$, and $\Lambda'=\zeta(\varepsilon\frac{2\pi}{a},0,\frac{2\pi}{c})$ in Fig. 9 nearby the c axis in order to study the transition from the region of nonadiabatic to adiabatic charge response together with the change in the mode behavior during this transition.

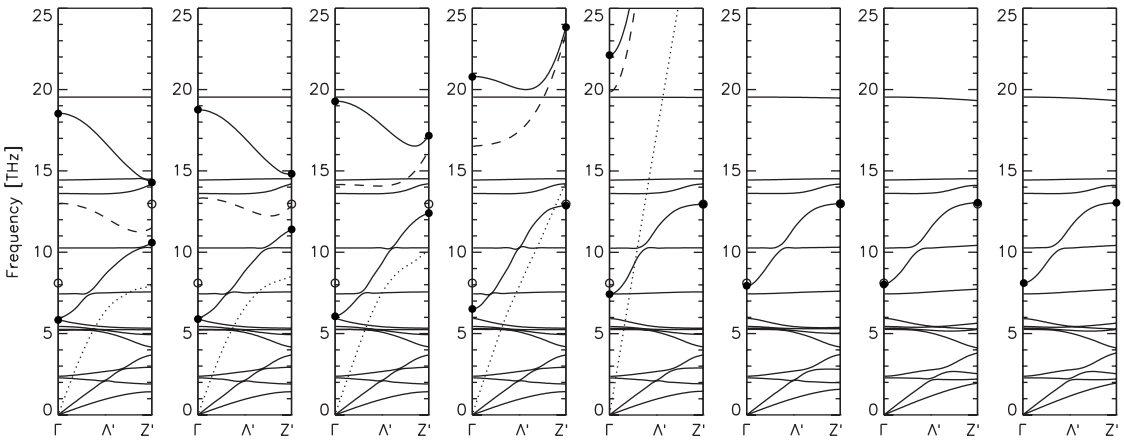

FIG. 9. Nonadiabatic coupled phonon-plasmon dispersion as calculated with model OP for the optimally doped state of La_2CuO_4 from Γ to $Z'=(\varepsilon\frac{2\pi}{a},0,\frac{2\pi}{c})$ along the $\Lambda'=\zeta(\varepsilon\frac{2\pi}{a},0,\frac{2\pi}{c})$ direction. In the different panels from left to right the following values for ε have been used: $\varepsilon=0.003,0.004,0.006,0.010,0.025,0.050,0.100$. The rightmost panel shows the result of a calculation within adiabatic approximation for $\varepsilon=0.100$. Only the Λ' branches (—) coupling to the charge fluctuations are shown. – –: free plasmon branch; ⋯: borderline for damping. Dots at Z': ● $O_z^{Z'}$(na), ○ $O_z^{Z'}$(ad). Dots at Γ: ● A_{2u}^{LO} (ferro, na); ○ A_{2u}^{TO} (ferro, ad). na: nonadiabatic; ad: adiabatic.

The frequency of the plasmon near Γ' in Fig. 8 is always very high and far outside the range of the phonon spectrum. Consequently the phonon dynamics is adiabatic in this **q**-space region. The phononlike nonadiabatic $O_z^{Z'}$ mode (lower full dot) converges to its adiabatic value (open circle) at about $\varepsilon=0.01$, while the plasmonlike $O_z^{Z'}$ mode (upper full dot) rapidly leaves the range of the spectrum. Simultaneously the dynamics becomes adiabatic. Compare with the calculation of the phonon dispersion in the rightmost panel where the static ($\omega=0$) approximation for $\Pi_{\kappa\kappa'}$ has been used. Likewise as in the investigations along the Δ' direction the nonadiabatic region can be characterized by $\varepsilon\approx 0.01$ and the present resolution limit for INS does not allow to resolve the mixed-phonon-plasmon dispersion. Only the result of averaging Λ'' between Γ' and Z' can be detected. In such a procedure the small nonadiabatic part close to the *c* axis will be outweighed in the measurement by a significant larger part where the dispersion is nearly adiabatic. In particular we extract the development of the dispersion which leads to the steep Λ_1 branch along Λ found in our calculations in the adiabatic limit. From this discussion it becomes clear how the measured data points in Fig. 2 should be interpreted, namely, as an average over the coupled mode dispersion with a dominant adiabatic contribution.

The calculated results in Fig. 8 qualitatively agree with the corresponding results in Ref. 14 in case the soft-plasmon limit is assumed. Concerning the steep Λ_1 branch the same conclusion can be drawn from the inspection of the calculated results along the Λ' direction displayed in Fig. 9. Again the phononlike $O_z^{Z'}$ mode matches the adiabatic result at about $\varepsilon\approx 0.01$ and the dispersion is virtually adiabatic with larger ε values. At the Γ-point two coupling longitudinal A_{2u} modes (full dots) occur which we denote as ferroelectric modes (FM) because of their intrinsic displacement patterns where the oxygen anions are vibrating coherently against the cations in the lattice. As a consequence the electric dipole moments generated by the motion add constructively to a large value. So, we can expect a large oscillator strength and as seen in the experiments[17] the FM dominates the infrared response for polarization along the *c* axis not only in the insulating state of La_2CuO_4 but also in the well doped metallic state. Such an optical activity in the *metallic* phase cannot be explained using the adiabatic approximation for the calculation of the phonon dispersion as is usually done by applying static DFT for the metal, because there will be no LO-TO splitting (A_{2u} splitting in the present case) being a measure of the oscillator strength. In such calculations the transverse effective charges vanish in the metallic state and consequently the induced dipole moments defining the oscillator strengths in the dielectric function (matrix) vanish, too. So, there will be no optical activity by the phonons. Moreover, when judging the findings in Refs. 25 and 52 of a small phonon contribution to the photoemission kink detected by ARPES (Refs. 53 and 54) one should keep in mind that these very interesting calculations also have been performed within static DFT, neglecting, e.g., the strong nonadiabatic dynamically screened polar coupling around the *c* axis and also correlation effects beyond LDA. On the other hand, the importance of the electron-phonon interaction in context with the kink in the dispersion of the nodal quasiparticles is emphasized in Ref. 55 on the basis of the two-dimensional three-band Hubbard model with electron-phonon interaction included and also in Ref. 56.

The observed infrared response in the metallic phase can be understood from our nonadiabatic results in Fig. 9. Here we find a very large A_{2u} splitting for the longitudinal plasmonlike FM (upper full dot at Γ) at 18.41 THz and the corresponding transverse FM (open circle at Γ) with a calculated frequency of 8.1 THz to be compared with 7.4 THz in the experiments,[37] respectively. Simultaneously, there is a smaller splitting between the latter mode and the longitudinal phononlike FM (lower full dot at Γ) at 5.80 THz. With increasing ε, i.e., when approaching the region of adiabatic charge response, the LO-TO splitting is closed from *below* and the plasmonlike branch with the plasmonlike FM at Γ and the plasmonlike $O_z^{Z'}$ mode at Z' rapidly disappears out of the phonon spectrum. Moreover, the phonon dispersion becomes adiabatic and the signature of the steep Λ_1 branch appears in the Λ' direction.

Summarizing, it should be emphasized that the presence of the large nonlocal long-ranged polar nonadiabatic electron-phonon coupling, which leads to the phonon-plasmon scenario, is also reflected in the measured infrared response. In Fig. 10 we show the calculated nonadiabatic phonon-plasmon dispersion of the Λ_1 modes displaying mode splitting along the $\Lambda\sim(0,0,1)$ direction. The full dots at Γ and *Z* represent the coupled phononlike (lower dot) and plasmonlike A_{2u} FM (upper dot) and the phononlike (lower dot) and plasmonlike (upper dot) O_z^Z mode, respectively. The calculated longitudinal plasmonlike A_{2u} FM at 18.41 THz is not far away from the experimental result for the longitudinal A_{2u} FM of La_2CuO_4 in the insulating state obtained with INS at about 17.5 THz. Of course the large splitting between this mode and the corresponding TO mode (open dot) accounts for the dominance of the FM in the infrared response also in the insulating state.[17,37] It should be remarked that in order to obtain the calculated dispersion curves the effect of the DF's is important. The latter considerably reduce the frequency of the plasmon as compared with the calculation which takes only CF's into account. This effect has already be demonstrated in Refs. 14 and 15.

From our preceding discussion of the coupled mode scenario along the Λ' and Λ'' direction it can be concluded that the branch with the phononlike FM at Γ and the phononlike $O_z^{Z'}$ mode at Z' converges to the steep Λ_1 branch of Fig. 10 in the Λ direction when approaching the adiabatic limit. Thereby the LO-TO splitting at Γ is closed from below and the phononlike O_z^Z mode reaches its adiabatic value. The plasmonlike branch connecting the corresponding plasmonlike modes at Γ and Z' rapidly leaves the phonon spectrum as can be seen in Fig. 9. The results as displayed in Figs. 8 and 9 as well as the interpretation of the massive line broadening for the O_z^Z are in general qualitative similar with corresponding results as obtained in the simplified model approach in Refs. 14 and 15 in case the extreme anisotropic soft-plasmon limit is assumed. However, for small values of ϵ in the Λ' direction noticeable differences arise. Moreover, along the Λ direction the phononlike mode with the steep

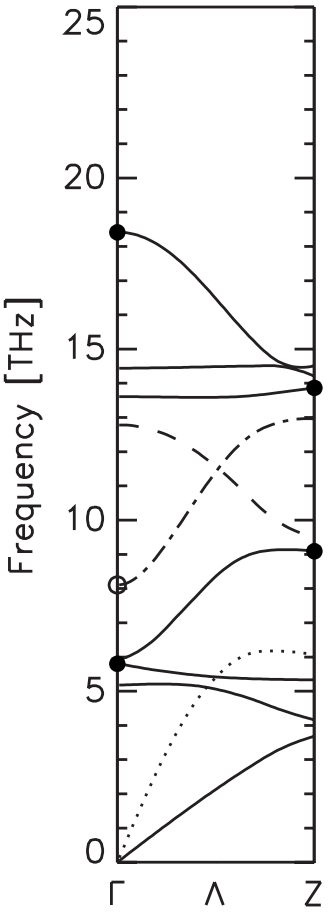

FIG. 10. Calculated nonadiabatic coupled phonon-plasmon dispersion of the Λ_1 modes of model OP for the optimally doped state of La_2CuO_4 along the $\Lambda \sim (0,0,1)$ direction. The coupling modes at Γ [A_{2u}^{LO} (ferro, na)] and at $Z(O_z^Z)$ are shown as black dots (●). The open dot (○) at Γ indicates A_{2u}^{TO} (ferro, ad).—: Λ_1 modes; – –: free plasmon branch; ···: borderline for damping; – · –: steep Λ_1 branch in the adiabatic approximation.

dispersion seen in Fig. 10 is not present at all in the earlier model. These facts underline again that the correct k_z dispersion is crucial for a save description of the phonon-plasmon scenario.

Of course, the position of the free plasmon along the c axis may differ in other cuprates from the situation found for La_2CuO_4 in the M31BM. We have studied parametrically the effect of a varying anisotropy in Refs. 14 and 15. For an assumed very weak interlayer coupling the resulting nonadiabatic dispersion in the metallic state along the Λ direction virtually cannot be distinguished from the dispersion of the (adiabatic) insulator and the optical phonon modes remain practically unscreened while increasing the coupling to what can be expected in a typical LDA-like calculation leads to an adiabatic charge response along the c axis.

As far as the pairing channel via coupled phonon-plasmon modes is concerned it is interesting to remark that the total effective interaction between the electrons via phonon-plasmon exchange is *attractive* in the frequency range between the transverse A_{2u} FM and the longitudinal plasmon-like A_{2u} FM at the Γ point. Thus, the very large splitting of this mode, see Figs. 9 and 10, is favorable for pairing and the role played in this game by the incomplete dynamical screening of the (bare) polar Coulomb interaction in the nonadiabatic region becomes evident. Note in this context that in recent work[6] it is found that the phonon-plasmon mechanism contributes constructively and significantly to the superconductivity in the cuprates and that the long-range polar electron-phonon interaction is important for pairing.[47,48]

For the modes propagating in the CuO plane virtually no changes can be observed when passing from the nonadiabatic treatment to the adiabatic calculation. The reason is the fast electron dynamics in the CuO plane as compared to the dynamics perpendicular to the plane; see Table I. From all the modes propagating in the CuO layer studied, the full oxygen breathing mode, O_B^X, shows the largest deviation, namely, a stiffening of 0.284 THz (9.47 cm^{-1}) for optimally doped La_2CuO_4 in the nonadiabatic treatment. We attribute this increase in the frequency to a *dynamical* reduced nesting effect with wave vectors around $X=\frac{\pi}{a}(1,1,0)$. Such an interpretation is consistent with the calculated FS in Fig. 5(a) and the maximum found at the X point for the reduced electronic polarizability function $\Pi_0(\mathbf{q})$ from Eq. (18). The change in the FS topology upon doping from holelike to electronlike and the related change in the nesting structures in Fig. 5 leads in the calculations to a reduction in the nonadiabatic stiffening of O_B^X [model OD1: 0.193 THz (6.44 cm^{-1}), model OD2: 0.059 THz (1.97 cm^{-1})].

A possible effect of the nonadiabatic charge response on the Raman modes in La_2CuO_4 could be quite interesting because very recently giant nonadiabatic effects in layered metals such as graphite intercalated compounds, which are three-dimensional metals with a considerable anisotropy along one direction, have been predicted in Ref. 57. Contrarily, in our calculations for La_2CuO_4 practically no nonadiabatic effects have been found for the Raman modes.

C. Phonon-plasmon-induced charge response and self-consistent changes in the potential

The induced charge redistribution for O_z^Z calculated in the adiabatic limit has been addressed shortly in Sec. III B and will be compared explicitly in Fig. 11 with the corresponding results as obtained in the nonadiabatic calculation. So far we can say that the phonon anomalies, i.e., the oxygen half breathing mode $\Delta_1/2$ and the full oxygen breathing mode O_B^X discussed if Refs. 15, 58, and 59 reflect the importance of the short-ranged part of the Coulomb interaction (U_d) while O_z^Z is specifically governed by the long-ranged part.

We now investigate the phonon-induced nonadiabatic charge response in optimally doped La_2CuO_4 represented by the model OP. The nonlocal, nonrigid part of the charge response related to the nonlocal EPI effects as excited by a phonon with wave vector $\mathbf{q}$ and polarization σ is given by

$$\delta\rho_n(\mathbf{r},\mathbf{q}\sigma) = \sum_{\mathbf{a},\kappa} \delta\zeta_\kappa^{\mathbf{a}}(\mathbf{q},\sigma)\rho_\kappa(\mathbf{r}-\mathbf{R}_\kappa^{\mathbf{a}}). \tag{22}$$

The CF's $\delta\zeta_\kappa^{\mathbf{a}}$ are obtained from Eq. (11) and the form-factors ρ_κ from Eq. (2).

In the contour plots of Fig. 11 the displacement induced rearrangement of the charge density according to Eq. (22) is

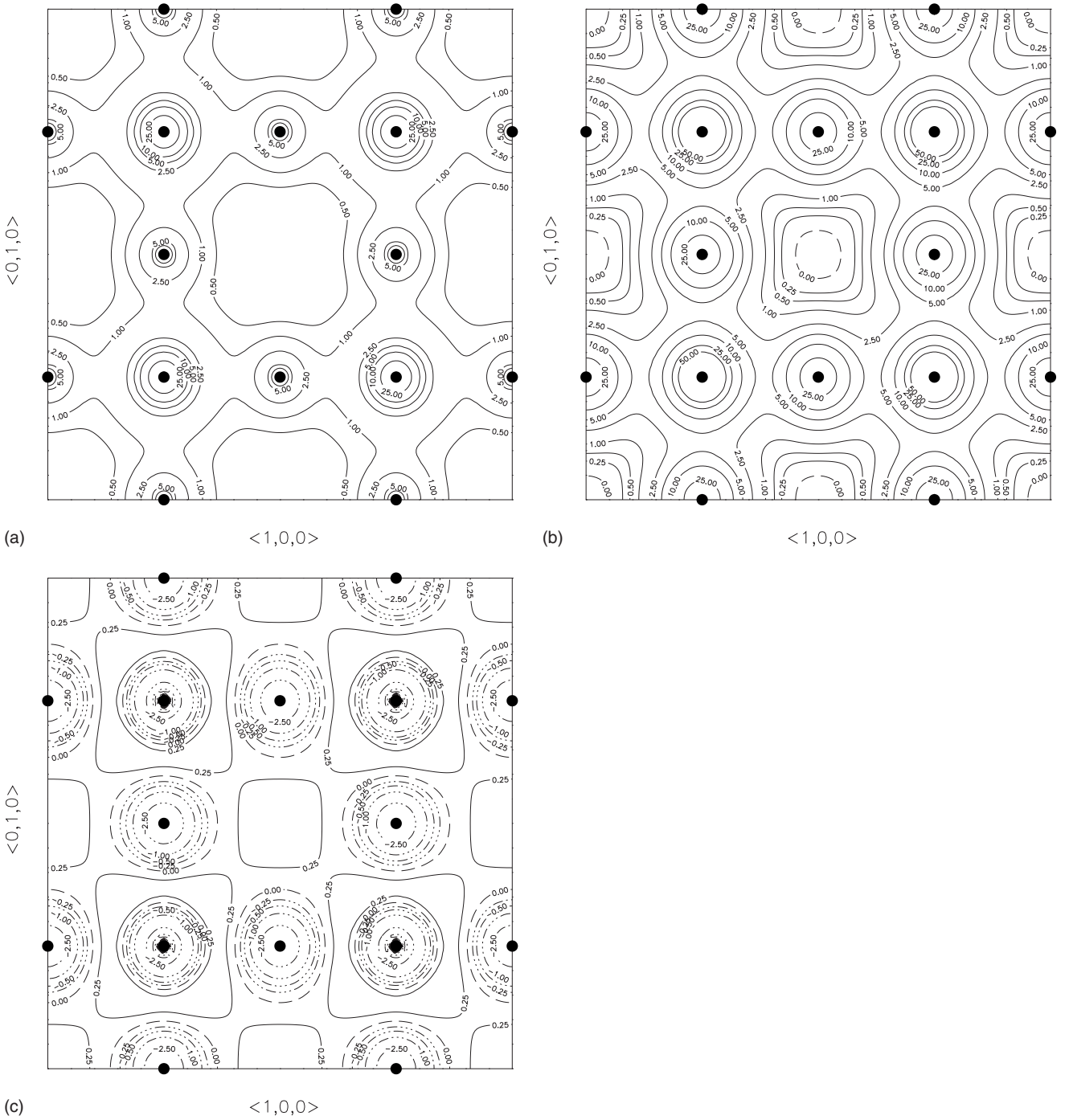

FIG. 11. Contour plot in the CuO plane of the nonlocal part of the displacement-induced charge-density redistribution for the O_z^Z mode in metallic La_2CuO_4 calculated according to Eq. (22) in adiabatic approximation for the M31BM (model OP) for the proper polarization part (a). (b) Same as in (a) but for the nonadiabatic phononlike O_z^Z mode. (c) Same as (a) but for the nonadiabatic plasmonlike O_z^Z mode. The units are in $10^{-4}\ e^2/a_B^3$. The phase of O_z^Z is as shown in Fig. 12. Full lines (—) mean that electrons are accumulated in the corresponding region of space and the broken dotted lines (–···–) indicate regions where the electrons are pushed away.

shown for the O_z^Z mode. The calculation has been performed for the model OP. Figure 11(a) displays the result for the adiabatic approximation and Figs. 11(b) and 11(c) picture the nonadiabatic result for the phononlike and plasmonlike O_z^Z modes, respectively. The phase of the vibration of the ions is as in Fig. 12, i.e., the apex oxygen move away from the CuO layer. The full lines ($\delta\rho_n > 0$) indicate that electrons are accumulated in the associated region of space, the broken dotted lines ($\delta\rho_n < 0$) mean that electrons are depleted in this region.

As already mentioned in Sec. III B and displayed explicitly in Fig. 11(a) in the adiabatic approximation O_z^Z (12.96 THz) generates CF's at the Cu and O_{xy} ions of the same sign in the whole CuO layer. In the adjacent layers the induced CF's are the same in magnitude but of opposite sign; compare with Fig. 12(a). Thus, O_z^Z activates an interlayer charge

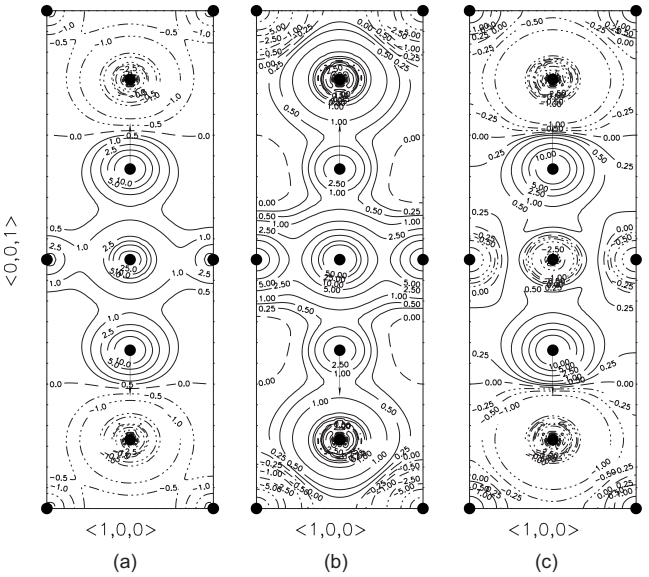

FIG. 12. Contour plot perpendicular to the CuO plane of the nonlocal part of the displacement-induced charge-density redistribution for the O_z^Z mode in La_2CuO_4 calculated from Eq. (22) in adiabatic approximation for the M31BM (model OP) (a). (b) Same as (a) but for the nonadiabatic phononlike O_z^Z mode. (c) Same as (a) but for the nonadiabatic plasmonlike O_z^Z mode. The units and the meaning of the line types are as in Fig. 11. The arrows denote the displacements of the apex oxygen ions.

transfer which is instantaneous in adiabatic approximation. Such a nonlocally excited screening process is very effective for screening the changes in the Coulomb interaction generated by the displacement of the apex oxygen ions and explains accordingly the large softening of O_z^Z during the insulator-metal transition.

Figure 11(b) records our calculated results for the nonadiabatically induced CF's of the phononlike O_z^Z mode in the CuO plane at 9.09 THz. In the nonadiabatic regime the electrons cannot follow instantaneously the movement of the ions. The now dynamically excited CF's at Cu and O_{xy} have the same sign in the CuO layer. The sign is as in the adiabatic case because the frequency of the free plasmon at Z is (slightly) higher (9.5 THz) than the phononlike O_z^Z mode. The magnitude of the CF's is considerably larger in the nonadiabatic case; see also Table III.

The interlayer CT is now of dynamic nature because of the dynamical screening of the Coulomb interaction and consequently a coupled collective phononlike excitation propagating along the c axis is created leading to the *correlated* charge rearrangement between the layers due to the *coherent* dynamics as shown in the snapshot of Fig. 12(b). Comparing with the adiabatic limit besides the strongly enhanced charge response, which explains the lower frequency, the sign of the CF's at the La ion has changed as compared with the adiabatic calculation. This correlates well with the change in sign of the displacement amplitude for La; compare with Table II. On the other hand, the sign of the CF's at the La for the plasmonlike mode is the same as in the adiabatic case in agreement with the same sign of the displacement of La in both calculations.

The coupled plasmonlike O_z^Z mode at 13.86 THz has a higher frequency than the free plasmon and apparently the charge response runs out of phase; see Fig. 11(c). This results in an *antiscreening* consistent with the higher mode frequency. The sign of the CF's at Cu and O_{xy} is not only opposite to that in the adiabatic and phononlike case but also smaller in magnitude (Table III). Figure 11(c) together with Fig. 12(c) give a snapshot of the collective plasmonlike interplane charge excitations being out of phase with the lattice and also strongly reduced in magnitude as compared with the phononlike excitation displayed in Figs. 11(b) and 12(b), respectively. As far as a calculation for the phonon plasmon induced charge response for O_z^Z is concerned no comparison can be made with our simplified model because this quantity has not been calculated before.

In order to get an impression for the displacement induced changes in the CF's $\delta\zeta_\kappa^{\mathbf{a}}(\mathbf{q},\sigma)$ according to Eq. (11) and the corresponding induced orbital averaged changes in the potential felt by the electrons $\delta V_\kappa^{\mathbf{a}}(\mathbf{q},\sigma)$ from Eq. (14), when passing from the region with a nonadiabatic dynamic charge response to the region with practically static adiabatic charge response, we display in Figs. 13(a) and 13(b) our calculated results for the phononlike $O_z^{Z'}$ mode along the Δ' direction; compare with Fig. 7(a). The calculations have been carried out for the optimally doped case using model OP and for the most important Cu $3d$ and O_{xy} $2p$ orbitals, respectively. Similar as for the phonon frequencies in Fig. 7(a) $\delta\zeta_\kappa$ and δV_κ converge beyond $\varepsilon \approx 0.01$ to their values in the adiabatic limit. Taking, for example, the calculated numbers at $\varepsilon = 0.00$ and 0.02, respectively, we recognize that the nonlocally excited CF's and in particular the nonlocally induced orbital averaged changes in the potential being a measure of the long-ranged polar coupling of the electrons and phonons

TABLE III. Magnitudes of the charge fluctuations $\delta\zeta_\kappa$ [Eq. (11)] and orbital-averaged changes in the self-consistent changes in the crystal potential δV_κ [Eq. (14)] of the OBSM as calculated with model OP for the Cu $3d$ and the O $2p$ orbitals in the CuO plane. $\delta\zeta_\kappa$ is given in units of 10^{-3} particles and δV_κ in units of meV. na: nonadiabatic; ad: adiabatic; ph: phononlike; pl: plasmonlike. The phase of the displacements for the OBSM is chosen in such a way that the oxygen is moving outward from the copper. $\delta\zeta_\kappa < 0$ means an accumulation of electrons in the corresponding orbital. $\delta V_\kappa > 0$ indicates that the region around the ion is attractive for electrons.

	O_z^Z(ad)		O_z^Z(na,ph)		O_z^Z(na,pl)		O_B^X(ad)		$\Delta_1/2$(ad)		O_B^X(na)		$\Delta_1/2$(na)	
	Cu $3d$	O $2p$	Cu $3d$	O $2p$	Cu $3d$	O $2p$	Cu $3d$	O $2p$	Cu $3d$	O $2p$	Cu $3d$	O $2p$	Cu $3d$	O $2p$
$\delta\zeta_\kappa$	−6.59	−2.63	−34.12	−18.13	1.32	2.13	−16.45	0	−14.76	−1.44	−16.95	0	−14.76	−1.44
δV_κ	−15.77	58.67	−955.98	−515.98	241.34	207.04	−93.92	0	−73.06	55.14	−87.20	0	−73.13	55.08

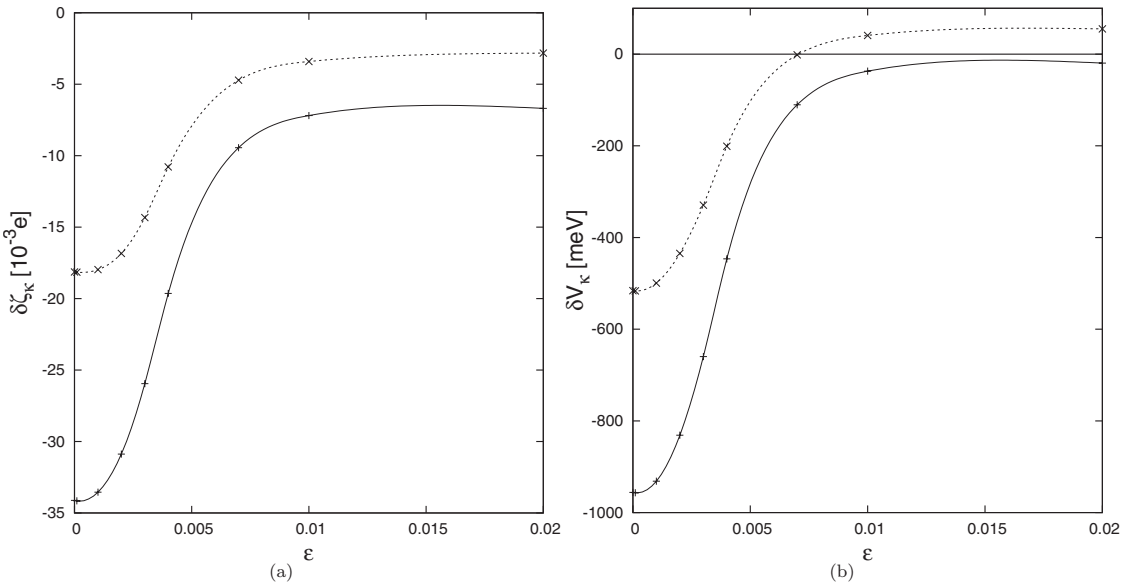

FIG. 13. (a) Calculated displacement-induced charge fluctuations $\delta\zeta_\kappa(\mathbf{q},\sigma,\omega)$ [Eq. (11)] and (b) corresponding orbital averaged changes in the crystal potential $\delta V_\kappa(\mathbf{q},\sigma,\omega)$ [Eq. (14)] for the phononlike $O_z^{Z'}$ mode along the Δ' direction $(\varepsilon\frac{2\pi}{a},0,\frac{2\pi}{c})$, $\varepsilon\in(0.00,0.02)$. Cu $3d$ (—) and $O_{xy}2p$ $(\cdots)$ orbital degrees of freedom are considered. The calculations have been performed for model OP.

are very strongly enhanced in the nonadiabatic region of phase space around the c axis; see also Table III.

The results for $\delta\zeta_\kappa$ and δV_κ differ quantitatively and qualitatively from the results in Ref. 15 confirming once again the importance of the correct k_z dispersion. Additionally, in Table III we summarize and compare the calculated orbital selective values of $\delta\zeta_\kappa$ and δV_κ for Cu $3d$ and O_{xy} $2p$ of the phonon anomalies $\Delta_1/2$, O_B^X, and O_z^Z, respectively. We extract already strong coupling of the adiabatic modes $\Delta_1/2$, O_B^X and of course the strong enhancement for the phononlike O_z^Z mode. This again points to the fact that besides the short-ranged part of the Coulomb interaction U_d being important for $\Delta_1/2$ and O_B^X, the strong long-ranged, nonlocal polar Coulomb interaction must play an important role in the normal and superconducting state of the doped cuprates.

Note that the $\Delta_1/2$ anomaly involves momentum transfer between nodal regions and could be important to understand the corresponding self-energy corrections, in particular, the nodal kink observed in ARPES experiments. Indeed, in a recent bulk-sensitive low photon energy ARPES study[60] it has been demonstrated that electron-phonon coupling is responsible for the nodal kink and the "half-breathing" mode $\Delta_1/2$ is the relevant mode.

In context with the very strong coupling of the *doping dependent* phononlike O_z^Z mode which is at 9.09 THz (37.6 meV) in model OP for the optimally doped state a special remark should be made. This mode involves momentum transfer between antinodal regions of the FS (similar as O_B^X or the resonant magnetic mode), however, with a drastically enhanced coupling strength as compared to O_B^X; see Table III. Consequently, this mode and of course $O_z^{Z'}$ should contribute to the electron self-energy via electron-phonon coupling in the antinodal region and possibly also to the antinodal pseudogap in the normal state. In sufficiently doped materials where a FS develops also in the antinodal region the geometry of the latter near the antinode (e.g., possible antinode nesting) should be important in context with the coupling via O_z^Z or $O_z^{Z'}$, respectively. In the superconducting state even an increased contribution to the self-energy via O_z^Z can be expected because of the large density of states enhancement in these regions due to the opening of a gap with d-wave symmetry.[61] Moreover, below T_C we will have a suppression of the low scattering rate of the electrons due to the opening of a gap and additionally below the finite energy of the phononlike mode.

This might be helpful to understand the dramatic change in line shape of the antinodal spectra seen in ARPES, where a sharp quasiparticle peak develops at the lowest binding energies followed by a dip and a broader hump. In the current literature these features are explained by a finite energy-collective bosonic mode which mostly is identified as the magnetic resonance mode.[62,63] On the other hand, the enhanced coherence of the quasiparticles at lower temperature in the superconducting state is simultaneously favorable for the existence of a phonon-plasmon scenario with the plasmonlike mode as another possibility for the collective bosonic mode.

As suggested in Ref. 64 *specific* modes (in particular $\Delta_1/2$) with a strong electron-phonon coupling can generate an *overscreening* of the intersite Coulomb interaction due to a phonon-induced charge transfer between Cu and O_{xy}. This strong coupling has been proposed in Ref. 64 to form a basis for the phonon mechanism of high-temperature superconductivity.

In case of cuprate superconductors with more than one CuO layer a qualitatively new possibility may arise as candidate for the finite energy collective bosonic mode. In these compounds additionally to the low-lying plasmon (intraband plasmon) of the single layer compounds discussed so far which results from a weak but nonvanishing k_z dispersion of the QP's an interband plasmon with a low energy can exist.

The latter emerges at vanishing k_z dispersion from a finite but small intralayer coupling, e.g., between the two CuO layers in a double layer system. Such a possibility has been investigated qualitatively for metallic $YBa_2Cu_3O_7$ within a simplified model approach; see Refs. 15 and 65.

Finally, we will make a few remarks concerning different possible contributions to pair binding in the cuprates taking into account the results from this work. The strong short-ranged repulsive U_d by itself does not help with the pair binding, however, favors *d*-wave symmetry and the usual argument then is that as an implication of a large U_d an antiferromagnetic exchange coupling J arises which leads to an attractive interaction between electrons of opposite spins on neighboring sites. U_d is an unretarded particle-particle interaction with no low-frequency dynamics and also the interaction related to J is unretarded.

On the other hand, several retarded attractive interactions mediated by virtual bosonic excitations with low-frequency dynamics are discussed in context with pairing in the cuprates. Most common are fluctuations of spin and/or charge degrees of freedom of the electron liquid and adiabatic phonons like $\Delta_1/2$ or O_B^X. From our findings in this paper low-frequency coupled phonon-plasmon modes resulting from the strong polar long-ranged interaction in the nonadiabatic region should be added to the list.

Concerning the possible importance of the contribution of the *c*-axis phonon plasmon modes to pair binding in the cuprates two aspects which may compete against each other should be considered. On one hand, the mode coupling is significantly enhanced as compared to the coupling of the adiabatic phonons discussed in context with the HTSCs (see, e.g., Table III), while on the other hand, the phase space around the *c* axis is small according to our findings. The latter fact of course also holds true if specific adiabatic phonons are considered and also for the magnetic resonance mode often thought to be relevant for pairing in the cuprates.

It still remains an open question which contribution and what kind of cooperation between the different players is most important for pairing and superconductivity in the cuprates. It seems that the high-energy as well as the low-energy scale is essential for a synergetic interplay of charge-spin and lattice degrees of freedom which underlies the physics in the cuprates in the normal as well as in the superconducting state.

IV. SUMMARY AND CONCLUSIONS

We have developed a realistic description of the electronic band structure of La_2CuO_4 and shown that a very accurate electronic dispersion along the *c* axis is crucial to calculate the wave vector and frequency-dependent proper polarization part of the DRF for the optimally to overdoped state. The latter is used to calculate the adiabatic and nonadiabatic charge response and the coupled mode dynamics in La_2CuO_4.

The large anisotropy along the *c* axis of the electronic structure of the cuprates is considerably underestimated in DFT-LDA calculations. So we have modified a LDA-based 31BM to account for the much weaker interlayer coupling in the real material. We have optimized the interlayer coupling in such a way that significant features of the Λ_1 phonons polarized parallel to this axis are well described. The Λ_1 modes have been chosen because they have proven to be highly sensitive in respect to the charge response orthogonal to the CuO plane.

Within the M31BM the measured Fermi surfaces for optimally and overdoped La_2CuO_4 are well described. Clearly visible in the experiments and the calculations is the change in the FS topology and of the nesting structures upon doping. The latter are shown to be reflected in the (noninteracting) susceptibility. Moreover, relevant Fermi-surface parameters for transport such as the Drude plasma energy tensor and the Fermi velocity tensor have been calculated and compared with standard LAPW calculations. An enhancement of about a factor of 5 for the anisotropy ratio is found for both types of parameters in the M31BM.

In our calculation of the phonon dispersion of the *c*-axis polarized Λ_1 modes dramatic changes occur between the adiabatic limit based on a static DRF and the nonadiabatic calculation founded on a dynamic DRF. The former leads to static and the latter to dynamic screening of the Coulomb interaction. On the other hand, virtually no nonadiabatic effects have been detected for the phonons propagating in the main symmetry direction Δ and Σ in the CuO plane. This is due to the fast dynamics of the electrons in the CuO layer as compared with the slow dynamics perpendicular to the plane. Only the planar oxygen breathing mode O_B^X experiences a minor nonadiabatic correction worth mentioning which we attribute to dynamical reduced nesting.

The adiabatic approximation as a basis paradigm to investigate lattice vibrations fails severely in a small sector of $\mathbf{q}$ space around the Λ direction. The large nonadiabatic effect found for the Λ_1 modes results from a low-lying *c*-axis plasmon predicted within the M31BM. This collective mode couples via the strong long-ranged polar Coulomb interaction to the optical phonons of allowed symmetry. In particular we have shown that the large softening of the O_z^Z mode during the insulator-metal transition and its giant linewidth found experimentally can be well understood in the phonon-plasmon scenario.

At the Γ point we identify ferroelectriclike A_{2u} modes with a large LO-TO splitting in form of plasmonlike and phononlike excitations. As seen in the experiments the ferroelectriclike A_{2u} mode dominates the infrared response for polarization along the *c* axis not only in the insulating state of La_2CuO_4 but also in the well doped metallic state. Such an optical activity also found in our nonadiabatic calculations for the metallic phase cannot be explained using the adiabatic approximation with static screening for the calculation of the phonon dispersion. This is what has been routinely done in the literature in first-principles calculations within static DFT. So, the latter are not consistent with experimental evidence concerning the *c*-axis response.

We have calculated the induced charge response of the strongly coupling apex oxygen stretching mode O_z^Z in the adiabatic limit and the nonadiabatic phonon-plasmon regime. Additionally we have computed the associated orbital averaged changes in the potential felt by the electrons when passing from the nonadiabatic phonon-plasmon region to the

adiabatic regime. Comparing with the adiabatic result we find for the phononlike O_z^Z mode a strongly enhanced in-phase charge response and accordingly a lower frequency appears while for the plasmonlike mode with a higher frequency the charge response is significantly weaker and runs out of phase, i.e., we observe an antiscreening effect.

The related changes in the orbital averaged potential have been calculated for the coupled phonon-plasmon modes. In particular for the phononlike mode we have calculated a very strong enhancement in the nonadiabatic sector of phase space. The possible importance of the phononlike O_z^Z mode for the electron self-energy has been pointed out. This demonstrates again the importance of the long-ranged polar coupling of the electrons and the *c*-axis phonons. As far as the low energy scale and the bosonic glue to keep the electron pairs in the cuprates together is concerned our calculations show that phonon-plasmon modes from the nonadiabatic zone around the *c* axis have to be added to the list of possible players.

Whenever possible, we have discussed the changes brought about by the improvements of the present model as compared with our earlier approach.

*falter@uni-muenster.de

[1] J. Ruvalds, Phys. Rev. B **35**, 8869 (1987).
[2] V. Z. Kresin and H. Morawitz, Phys. Rev. B **37**, 7854 (1988).
[3] A. Griffin and A. J. Pindor, Phys. Rev. B **39**, 11503 (1989).
[4] H. A. Fertig and S. Das Sarma, Phys. Rev. B **44**, 4480 (1991).
[5] S.-M. Cui and C.-H. Tsai, Phys. Rev. B **44**, 12500 (1991).
[6] A. Bill, H. Morawitz, and V. Z. Kresin, Phys. Rev. B **68**, 144519 (2003).
[7] I. Bozovic, Phys. Rev. B **42**, 1969 (1990).
[8] L. Hedin and J. D. Lee, Phys. Rev. B **64**, 115109 (2001).
[9] R. Gajic, E. K. H. Salje, Z. V. Popovic, and H. L. Dewing, J. Phys.: Condens. Matter **4**, 9643 (1992).
[10] R. S. Markiewicz, M. Z. Hasan, and A. Bansil, Phys. Rev. B **77**, 094518 (2008).
[11] A. F. Ho and A. J. Schofield, Phys. Rev. B **71**, 045101 (2005).
[12] L. Pintschovius, Phys. Status Solidi B **242**, 30 (2004).
[13] L. Pintschovius and W. Reichardt, in *Physics and Chemistry of Materials with Low Dimensional Structures*, edited by A. Furrer (Kluwer, Dordrecht/Academic, New York, 1998), Vol. 20.
[14] C. Falter, G. A. Hoffmann, and F. Schnetgöke, J. Phys.: Condens. Matter **14**, 3239 (2002).
[15] C. Falter, Phys. Status Solidi B **242**, 78 (2004).
[16] S. Uchida, K. Tamasaku, and S. Tajima, Phys. Rev. B **53**, 14558 (1996).
[17] R. Henn, J. Kirchner, and M. Cardona, Physica C **269**, 99 (1996).
[18] R. Henn, A. Wittlin, M. Cardona, and S. Uchida, Phys. Rev. B **56**, 6295 (1997).
[19] S. Uchida, T. Ido, H. Takagi, T. Arima, Y. Tokura, and S. Tajima, Phys. Rev. B **43**, 7942 (1991).
[20] W. Meevasana, T. P. Devereaux, N. Nagaosa, Z.-X. Shen, and J. Zaanen, Phys. Rev. B **74**, 174524 (2006).
[21] A. S. Alexandrov, Phys. Rev. B **46**, 2838 (1992).
[22] S. Y. Savrasov and O. K. Andersen, Phys. Rev. Lett. **77**, 4430 (1996).
[23] C. Z. Wang, R. Yu, and H. Krakauer, Phys. Rev. B **59**, 9278 (1999).
[24] K. P. Bohnen, R. Heid, and M. Krauss, Europhys. Lett. **64**, 104 (2003).
[25] F. Giustino, M. L. Cohen, and S. G. Louie, Nature (London) **452**, 975 (2008).
[26] C. Falter, Th. Bauer, and F. Schnetgöke, Phys. Rev. B **73**, 224502 (2006).
[27] Th. Bauer and C. Falter, Phys. Rev. B **77**, 144503 (2008).
[28] M. J. De Weert, D. A. Papaconstantopoulos, and W. E. Pickett, Phys. Rev. B **39**, 4235 (1989).
[29] N. E. Hussey, M. Abdel-Jawad, A. Carrington, A. P. Mackenzie, and L. Balicas, Nature (London) **425**, 814 (2003).
[30] S. Sahrakorpi, M. Lindroos, R. S. Markiewicz, and A. Bansil, Phys. Rev. Lett. **95**, 157601 (2005).
[31] C. C. Homes, S. V. Dordevic, D. A. Bonn, W. N. Ruixing, Liang Hardy, and T. Timusk, Phys. Rev. B **71**, 184515 (2005).
[32] Y. H. Kim, P. H. Hor, X. L. Dong, F. Zhou, Z. X. Zhao, Z. Wu, and J. W. Xiong, Phys. Rev. B **71**, 092508 (2005).
[33] C. Falter, M. Klenner, and W. Ludwig, Phys. Rev. B **47**, 5390 (1993).
[34] C. Falter, M. Klenner, G. A. Hoffmann, and F. Schnetgöke, Phys. Rev. B **60**, 12051 (1999).
[35] C. Falter, Phys. Rep. **164**, 1 (1988).
[36] C. Falter, M. Klenner, and G. A. Hoffmann, Phys. Rev. B **52**, 3702 (1995).
[37] C. Falter and F. Schnetgöke, Phys. Rev. B **65**, 054510 (2002).
[38] J. P. Perdew and A. Zunger, Phys. Rev. B **23**, 5048 (1981).
[39] H. Krakauer, W. E. Pickett, and R. E. Cohen, J. Supercond. **1**, 111 (1988).
[40] M. J. Litzkow, M. Livny, and M. W. Mutka, *Condor—A Hunter of Idle Workstations*, Proceedings of the Eighth International Conference on Distributed Computing Systems (IEEE Computer Society, Washington, DC, 1988), p. 104.
[41] C. Falter, M. Klenner, and G. A. Hoffmann, Phys. Status Solidi B **209**, 235 (1999).
[42] T. Yoshida, X. J. Zhou, K. Tanaka, W. L. Yang, Z. Hussain, Z.-X. Shen, A. Fujimori, S. Sahrakorpi, M. Lindroos, R. S. Markiewicz, A. Bansil, S. Komiya, Y. Ando, H. Eisaki, T. Kakeshita, and S. Uchida, Phys. Rev. B **74**, 224510 (2006).
[43] T. Yoshida, X. J. Zhou, D. H. Lu, S. Komiya, Y. Ando, H. Eisaki, T. Kakeshita, S. Uchida, Z. Hussain, Z. X. Shen, and A. Fujimori, J. Phys.: Condens. Matter **19**, 125209 (2007).
[44] A. Bansil, M. Lindroos, S. Sahrakorpi, and R. S. Markiewicz, Phys. Rev. B **71**, 012503 (2005).
[45] P. B. Allen, W. E. Pickett, and H. Krakauer, Phys. Rev. B **36**, 3926 (1987).
[46] W. E. Pickett, Rev. Mod. Phys. **61**, 433 (1989).
[47] A. S. Alexandrov, J. Phys.: Condens. Matter **19**, 125216 (2007).
[48] T. M. Hardy, J. P. Hague, J. H. Samson, and A. S. Alexandrov, Phys. Rev. B **79**, 212501 (2009).
[49] W. Meevasana, N. J. C. Ingle, D. H. Lu, J. R. Shi, F. Baumberger, K. M. Shen, W. S. Lee, T. Cuk, H. Eisaki, T. P. De-

vereaux, N. Nagaosa, J. Zaanen, and Z.-X. Shen, Phys. Rev. Lett. **96**, 157003 (2006).
[50] L. Pintschovius (private communication).
[51] L. Pintschovius, D. Reznik, and K. Yamada, Phys. Rev. B **74**, 174514 (2006).
[52] R. Heid, K. P. Bohnen, R. Zeyher, and D. Manske, Phys. Rev. Lett. **100**, 137001 (2008).
[53] A. Lanzara, P. V. Bogdanov, X. J. Zhou, S. A. Kellar, D. L. Feng, E. D. Lu, T. Yoshida, H. Eisaki, A. Fujimori, K. Kishio, J.-I. Shimoyama, T. Noda, S. Uchida, Z. Hussain, and Z.-X. Shen, Nature (London) **412**, 510 (2001).
[54] P. D. Johnson, T. Valla, A. V. Fedorov, Z. Yusof, B. O. Wells, Q. Li, A. R. Moodenbaugh, G. D. Gu, N. Koshizuka, C. Kendziora, Sha Jian, and D. G. Hinks, Phys. Rev. Lett. **87**, 177007 (2001).
[55] S. Koikegami and Y. Aiura, Phys. Rev. B **77**, 184519 (2008).
[56] M. L. Kulic and O. V. Dolgov, Phys. Rev. B **76**, 132511 (2007).
[57] A. M. Saitta, M. Lazzeri, M. Calandra, and F. Mauri, Phys. Rev. Lett. **100**, 226401 (2008).
[58] C. Falter, M. Klenner, G. A. Hoffmann, and Q. Chen, Phys. Rev. B **55**, 3308 (1997).
[59] C. Falter and G. A. Hoffmann, Phys. Rev. B **61**, 14537 (2000).
[60] H. Iwasawa, J. F. Douglas, K. Sata, T. Masui, Y. Yoshida, Z. Sun, H. Eisaki, H. Bando, A. Ino, M. Arita, K. Shimada, H. Namatame, M. Taniguchi, S. Tajima, S. Uchida, T. Saitoh, D. S. Dessau, and Y. Aiura, Phys. Rev. Lett. **101**, 157005 (2008).
[61] W. S. Lee, S. Johnston, T. P. Devereaux, and Z. X. Shen, Phys. Rev. B **75**, 195116 (2007).
[62] M. R. Norman, H. Ding, J. C. Campuzano, T. Takeuchi, M. Randeria, T. Yokoya, T. Takahashi, T. Mochiku, and K. Kadowaki, Phys. Rev. Lett. **79**, 3506 (1997).
[63] A. Kaminski, M. Randeria, J. C. Campuzano, M. R. Norman, H. Fretwell, J. Mesot, T. Sato, T. Takahashi, and K. Kadowaki, Phys. Rev. Lett. **86**, 1070 (2001).
[64] M. Tachiki, M. Machida, and T. Egami, Phys. Rev. B **67**, 174506 (2003).
[65] G. A. Hoffmann, Ph.D. thesis, University of Münster, 2000.